
Università degli Studi di Urbino Carlo Bo

Department of Biomolecular Sciences

Ph.D. PROGRAMME IN: Sciences of Life, Health and Biotechnologies

CYCLE: XXXIV

CURRICULUM IN: Biochemical, Pharmacological and Biotechnological Sciences

# *Mechanism whereby arsenite promotes mitochondrial superoxide formation: critical regulation by upstream events resulting in $Ca^{2+}$ mobilization and mitochondrial accumulation*

**SSD: BIO/14**

**Coordinator**: Prof. Marco Rocchi

**Supervisor**: Prof. Orazio Cantoni

**Co-Supervisor**: Prof. Andrea Guidarelli

**Ph.D. student**: Alessia Catalani

ACADEMIC YEAR: 2020/2021

## *Abstract*

Arsenite is a widely distributed carcinogen and toxic compound that mediates various deleterious effects via the intermediate formation of reactive oxygen species (ROS). Recent work performed in our laboratory has demonstrated that prolonged (hours) exposure of human myeloid leukemia U937 cells to low micromolar concentrations of arsenite elicits $Ca^{2+}$ release from the inositol-1,4,5-trisphosphate receptor ($IP_3R$) and the crosstalk between this pool and the ryanodine receptor (RyR). The fraction of $Ca^{2+}$ derived from the RyR was then critical to promote the mitochondrial accumulation of the cation and the ensuing mitochondrial superoxide ($mitoO_2^{-\cdot}$) formation. It was interesting to observe that these time and concentration requirements were dramatically lowered under conditions in which the mitochondrial accumulation of $Ca^{2+}$ was enforced by $IP_3$ releasing or RyR agonists. Thus, very low concentrations of arsenite rapidly target the mitochondrial respiratory chain, with however significantly greater time and concentration requirements for $Ca^{2+}$ mobilization from the ER. Based on the above findings, this second event appears critical and likely restricted to cell types concomitantly expressing the $IP_3R$ and a RyR. This notion was clearly established in studies showing that arsenite fails to promote mitochondrial $Ca^{2+}$ accumulation and $mitoO_2^{-\cdot}$ formation in cells uniquely expressing the $IP_3R$. Arsenite instead elicited these events when cells were manipulated to gain expression of the RyR and lost these abilities under conditions in which cells expressing both $Ca^{2+}$ channels were manipulated to downregulate the RyR.

RyR expression therefore represents a critical requirement for mitochondrial $Ca^{2+}$ accumulation and $mitoO_2^{-\cdot}$ formation induced by arsenite. The second requirement is instead represented by the recruitment phase of this channel, apparently located in close apposition with the mitochondria. We found that,

under the above conditions, arsenite causes an ER stress response associated with a threefold increase in ER oxidoreductin 1α (ERO1α) levels in cells expressing both the $IP_3R$ and RyR. EN460, an inhibitor of ERO1α, recapitulated all the effects associated with RyR inhibition or downregulation, including prevention of RyR-induced $Ca^{2+}$ accumulation in mitochondria and the resulting mito$O_2^{-\cdot}$ formation. Moreover, ERO1α knockout cells responded to arsenite as their wild-type counterpart supplemented with EN460. As a final note, arsenite enhanced the expression of ERO1α via a mechanism mediated by $Ca^{2+}$ release from both the $IP_3R$ and RyR.

We therefore conclude that arsenite activates a positive feedback amplification cycle between $Ca^{2+}$ levels and ERO1α in the ER, by which $IP_3R$-dependent $Ca^{2+}$ induces ERO1α and ERO1α promotes $Ca^{2+}$ release *via* RyR, thereby amplifying the initial $Ca^{2+}$ load and causing the mitochondrial accumulation of the cation, critical for mito$O_2^{-\cdot}$ formation.

# Index

**1. Introduction……6**

**2. Materials and methods……12**

**2.1** Chemicals……..12

**2.2** Antibodies……..12

**2.3** Cell culture and treatment conditions……12

**2.4** DHR and MitoSOX Red fluorescence assay…….…….……14

**2.5** Measurement of intracellular free calcium levels and mitochondrial $Ca^{2+}$…….....…14

**2.6** Super resolution and confocal microscopy……15

**2.7** Immunofluorescence analysis……15

**2.8** Western Blot analysis…….……16

**2.9** Redox Western Blot analysis……..…17

**2.10** Fluorogenic Caspase 3 assay…….…..…..…17

**2.11** Analysis of apoptosis with Hoechst 33342 assay……....17

**2.12** Cytotoxicity assay……....18

**2.13** Alkaline Halo assay…….…18

**2.14** ATP determination……..18

**2.15** Measurement of GSH content by High-Performance Liquid Chromatography ……19

**2.16** Real-time quantitative RT-PCR analysis…….20

**2.17** Statistical analysis……....20

**3. Results and Discussion……...21**

**3.1** Arsenite-induced mitochondrial superoxide formation: time and concentration requirements for the effects of the metalloid on the endoplasmic reticulum and mitochondria……..……..21
**3.2** Functional organization of the endoplasmic reticulum dictates the susceptibility of target cells to arsenite-induced mitochondrial superoxide formation, mitochondrial dysfunction and apoptosis……...…32
**3.3** ERO1α mediates recruitment of the ryanodine receptor after inositol 1, 4,5-trisphosphate receptor stimulation induced by arsenite.....….45

**4. Conclusion……...……..51**

**5. References…….……55**

# 1. Introduction

Calcium ($Ca^{2+}$) is an almost universal intracellular messenger, controlling a diverse range of cellular processes as gene transcription, muscle contraction and cell proliferation. The ability of a simple ion as $Ca^{2+}$ to play a pivotal role in cell biology results from the facility that cells have to shape $Ca^{2+}$ signals in the dimensions of space, time and amplitude. To generate the variety of observed $Ca^{2+}$ signals, different cell types employ components selected from a $Ca^{2+}$ signaling 'toolkit', which includes an array of signaling, homeostatic and sensory mechanisms. By mixing and matching components from the toolkit, cells can obtain $Ca^{2+}$ signals that suit their physiology (Bootman et al., 2001).

Intracellular mobilization of $Ca^{2+}$, an event that regulates an array of different physiological functions, as well as pathologically and toxicologically relevant dysfunctions, is mediated predominantly by two $Ca^{2+}$ channels, the inositol 1,4,5-trisphosphate receptor ($IP_3R$) and the ryanodine receptor (RyR) (Berridge et al., 2016; Chernorudskiy and Zito, 2017; Meissner et al., 2017). These $Ca^{2+}$ channels are located on the surface of the endoplasmic reticulum (ER) and share numerous similarities, including a complex regulation mediated by reactive oxygen species (ROS) (Gorlach et al., 2015). RyR, a homotetramer comprising four 565 kDa monomers of approximately 5000 amino acids each (Zalk et al. 2015), is a member of the same gene family as $IP_3R$ and has evolved specialized functions required for excitation–contraction coupling in striated muscles. There are three subtypes of RyRs in mammalian tissues. RyR1 (Marks et al. 1989) and RyR2 (Brillantes et al. 1992), expressed in the skeletal and cardiac muscle, respectively, are also expressed in non-muscle tissues (Fitzgerald et al., 1994; Maki et al., 1996; Rosemblit et al., 1999) (Brillantes et al., 1994). RyR3, originally identified in the brain, but widely expressed in non-neuronal tissues (McPherson & Campbell, 1990; McPherson et al. 1991;

Hakamata et al. 1992; Kuwajima et al. 1992). RyRs are macromolecular complexes (Marks et al. 2002) specifically targeted to the channels' cytoplasmic domain to regulate its gating and activity. Stress induced remodeling of the complex contributes to disorders including muscular dystrophy, heart failure, cardiac arrhythmias and cognitive dysfunction (Marx et al., 2000, 2001; Santulli et al., 2017).

$IP_3R$ channels are homo- or hetero-tetramers composed of four subunits (approximately 300 kDa each). Three forms of $IP_3Rs$ (types 1, 2 and 3) have been described (Nakagawa et al., 1991). Virtually all cell types have at least one form of $IP_3R$ and many express all three types. $IP_3R2$ is the predominant isoform in contractile myocardial cells and in the sinoatrial node (Verma et al., 1992), whereas $IP_3R1$ is the more abundant in other cell types, including endothelial cells (ECs) and Purkinje fibers (Gorza et al., 1993). $IP_3R$ function is regulated by a classic second messenger cellular signaling pathway mediated by inositol 1,4,5-trisphosphate ($IP_3$), produced primarily by phospholipase C (PLC) metabolism of phosphoinositol-4,5-bisphosphate ($PIP_2$) in response to the stimulation of G-protein-coupled receptors. $IP_3Rs$ are also macromolecular signaling complexes that mediate phosphorylation by receptor tyrosine kinases and non-receptor tyrosine kinases, for instance protein kinase A (PKA), and are regulated during physiological and pathophysiological states (Marks et al., 1990, Moschella et al., 1995).

Arsenic is one of the most important global environmental pollutants and is a persistent bioaccumulative carcinogen (Sukhvinder Kaur et al., 2011). Ingestion of contaminated drinking water by populations from various parts of the planet has been associated with the induction of different types of tumors [lung, skin, liver, bladder and kidney (Sankpal et al., 2012; Shakoor et al., 2017; Zhou and Xi, 2018)] as well as other nonmalignant diseases affecting various tissues and organs (Flora, 2011; Shakoor et al., 2017).

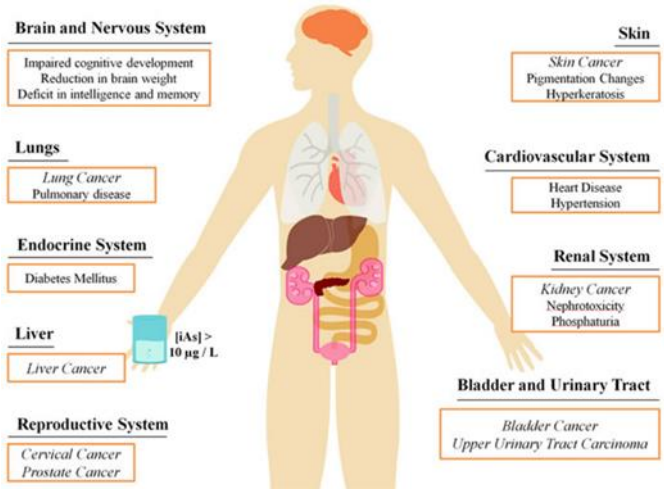


Arsenite causes a plethora of effects in target cells through its direct binding to biomolecules or *via* the intermediate formation of reactive oxygen species (ROS) (Flora 2011; Jomova et al., 2011). Unfortunately, the very large majority of the available studies provided a general indication of arsenite-induced ROS formation, with no systematic attempt to identify their origin and, thus, the overall scenario remains poorly understood (Hu et al. 2020). Hence, the impact of the metalloid in different cell types should depend on their susceptibility to arsenite-induced ROS formation, in turn affected by an array of variables associated with the specific characteristics of the cells, tissues, and organs. Arsenite induces various responses in different cell lines producing ROS *via* different mechanisms, *e.g.*, in the mitochondrial respiratory chain (Liu et al., 2005; Guidarelli et al., 2015, 2016), *via* NADPH oxidase activation (Smith et al., 2001; Chou et al., 2004; Straub et al., 2008), or through both mechanisms (Li et al., 2014).

In our laboratory, we used undifferentiated U937 (U-U937) cells and found that they respond to challenge with low concentrations of arsenite with the time-dependent formation of mitochondrial superoxide (mito$O_2^{-\cdot}$) (Guidarelli et al., 2015, 2016), sensitive to inhibitors of electron transport in

the respiratory chain. Furthermore, we also used respiration-deficient U937 (RD-U937 cells) and demonstrated their inability to generate mito$O_2^{-\cdot}$ after arsenite treatment. We then investigated the mechanism whereby arsenite mobilizes $Ca^{2+}$ from the endoplasmic reticulum (ER) and found that the metalloid promotes an initial slow mobilization of a limited amount of the cation from the $IP_3R$. This response was ROS-independent and possibly mediated by the direct interaction of arsenite with this $Ca^{2+}$ pool (Guidarelli et al., 2018). The initial $IP_3R$ stimulation was associated with the recruitment of the RyR, thereby leading to the release of large amounts of $Ca^{2+}$ (Guidarelli et al., 2018). This second response was therefore sensitive to RyR inhibitors and RyR downregulation achieved after differentiation (D-U937 cells) (Guidarelli et al., 2009).

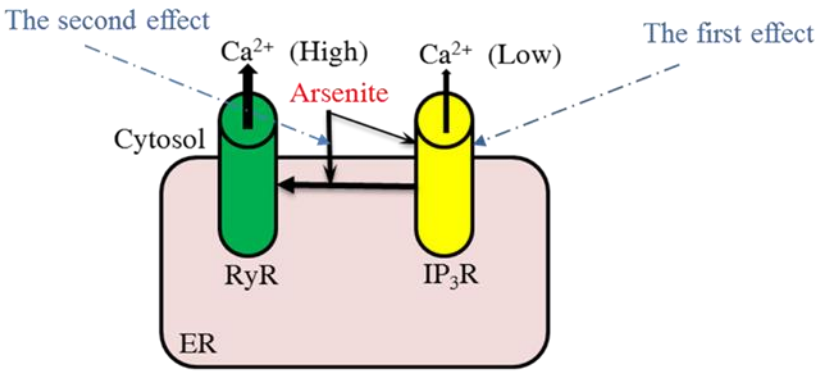


Guidarelli et al., J Pharmacol Exp Ther, 2018

Importantly, the fraction of $Ca^{2+}$ derived from the RyR was taken up by the mitochondria through the low affinity mitochondrial $Ca^{2+}$ uniporter (MCU) and was critical for mito$O_2^{-\cdot}$ formation (Guidarelli et al., 2019). Thus, mitochondrial ROS formation was sensitive to inhibitors of electron transport and the respiration-deficient phenotype as well as to $IP_3R$, RyR or

MCU inhibitors. In addition, the metalloid failed to promote mito$O_2^{-\cdot}$ formation in cells with downregulated RyR (Guidarelli et al., 2019).

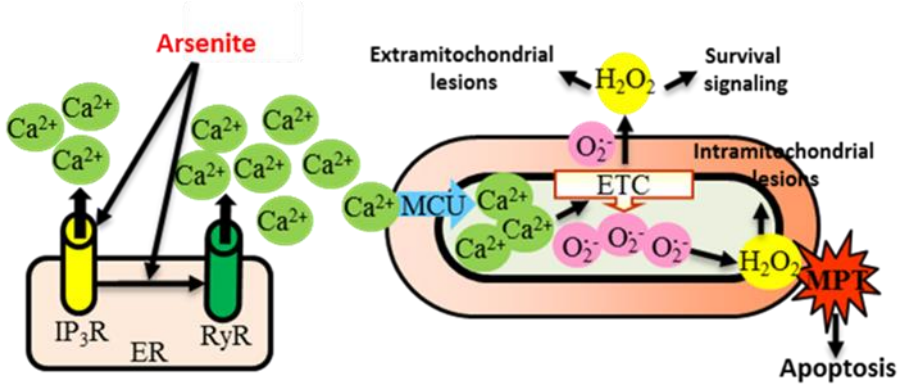


Guidarelli et al., Redox Biol, 2019

These observations and considerations stimulated the present thesis work in which we asked three specific questions. The first one was on the requirements (time and concentration) for arsenite in the overall process leading to mito$O_2^{-\cdot}$ formation. The second question was on the implication of our previous findings in terms of cell specificity. In other words, the mechanism whereby arsenite promotes mito$O_2^{-\cdot}$ formation in U-U937 cells implies that this response is restricted to cells with a specific spatial and functional organization of their ER, in particular with reference to the reciprocal topology of the two $Ca^{2+}$ release receptors, the $IP_3R$ and RyR, and their relative vicinity to mitochondria. It is indeed well established that contact sites between the ER and mitochondria regulate $Ca^{2+}$ transfer between these two organelles, through the MCU (Kirichok et al. 2004; Rizzuto et al. 2012), which requires cytosolic $Ca^{2+}$ concentrations ($[Ca^{2+}]_c$ in the 10-20 µM range. These high $[Ca^{2+}]_c$ can be reached only in the very close proximity of the $IP_3R$ or the RyR, when activated by agonist stimulation, or treatment with toxic compounds (Van Petegem 2012; Bansaghi et al. 2014;

Berridge 2016; Guidarelli et al. 2019). The aforementioned hypothesis initially build up on experiments performed in U-U937, RD-U937 and D-U937 cells, can therefore be challenged in other cell types characterized by a different spatial organization of the ER.

The third question addressed the issue of the mechanism(s) underlying the crosstalk between the $IP_3R$ and RyR after arsenite stimulation. We tested the possibility that the metalloid causes an ER stress associated with increased expression of ERO1α, a protein disulfide oxidase that might release $H_2O_2$ site-specifically, to oxidase critical thiols of the RyR and promote the release of $Ca^{2+}$.

## 2. Materials and methods

**2.1 Chemicals.** Sodium arsenite, 2-aminoethoxydiphenyl borate (2-APB), Ry, L-ascorbic acid (AA), rotenone, caffeine (Cf), ATP, phorbol-12-myristate 13-acetate (PMA), apocynin, diphenyleneiodonium (DPI), Hoechst 33342 and most of the reagent-grade chemicals were purchased from Sigma-Aldrich (Milan, Italy). Ru360, Fluo 4-acetoxymethyl ester (Fluo 4-AM), Rhod 2-acetoxymethyl ester (Rhod 2-AM), dihydrorhodamine 123 (DHR), and MitoSOX red were from Thermo Fisher Scientific (Milan, Italy). MitoTrackerDeep Red tracker was purchased from Molecular probes (Leiden, NL).

**2.2 Antibodies.** The antibodies against the phosphorylated or non-phosphorylated p47 phagocyte oxidase (anti-Phospho-p47$^{phox}$, SAB4504721; anti-p47$^{phox}$, SAB4502810) were purchased from Sigma-Aldrich (Milan, IT). Antibody against actin (anti-actin, VMA00048) was acquired from BIO-RAD (Hercules, CA). The antibody against ERO1L was generated as indicated in (Zito et al., 2010). The antibody against thioredoxin-2 (anti-Trx2; sc-133201), against cytochrome c (anti-Cyt c, 7H8, sc-13560) and the horseradish peroxidase–conjugated secondary antibody (anti-rabbit IgG-HRP, sc-2357; anti-mouse-IgGk BP-HRP, sc-516102) were obtained from Santa Cruz (Santa Cruz, CA).

**2.3 Cell culture and treatment conditions.** U937 human myeloid leukemia cells, herein defined as U-U937 cells, were cultured in suspension in RPMI 1640 medium (Sigma-Aldrich, Milan, IT). Culture media were supplemented with 10% fetal bovine serum (FBS, Euroclone, Celbio Biotecnologie, Milan, IT), penicillin (100 U/ml), and streptomycin (100 mg/ml) (Euroclone). Cells were grown at 37°C in T-75 tissue culture flasks (Corning Inc., Corning, NY) gassed with an atmosphere of 95% air and 5% $CO_2$. These cells were differentiated to monocytes (*i.e.*, D-cells) by 4 days

of growth in culture medium supplemented with 1.3% dimethylsulfoxide (Guidarelli et al., 2009). The respiration-deficient phenotype (*i.e.*, RD-U937) was obtained by culturing U937 cells in RPMI medium containing 110 μg/ml pyruvate, 5 μg/ml uridine and 400 ng/ml ethidium bromide for 4 days with medium changes every 2 days (Guidarelli et al., 2016).

The mouse myoblast cell line C2C12 (ECACC 91031101, lot 12F005) was purchased from the European Collection of Authenticated Cell Cultures (ECACC, Salisbury, UK) and cultured in high-glucose D-MEM (Sigma-Aldrich) supplemented with 10% heat inactivated FBS, 2 mM L-glutamine (Euroclone). Cells at 60-70 % confluence were split 1:4 or 1:5. Upon 80-90% confluence, C2C12 myoblasts (*i.e.*, U-C2C12) were stimulated to differentiate (*i.e.*, D-C2C12) by changing the growth medium with D-MEM containing 1% heat inactivated FBS. Fresh D-MEM (1% heat inactivated FBS) was replaced daily. In all experiments reported in the present work, C2C12 cells were used up to passage number 15.

ERO1α KO C2C12 were generated with the CRISPR/CAS9 technology (sc-401747-HDR, Santa Cruz Biotechnology) (Varone et al., 2019). ERO1 KO C2C12 and the WT counterparts were cultured and differentiated as described above.

HeLa human cervical cancer cells were grown in Dulbecco's modified Eagle medium supplemented with 10% FBS (Euroclone). All cells were cultured with penicillin (100 units/ml) and streptomycin (100 mg/ml) (Euroclone) at 37°C in T-75 tissue culture flasks (Corning) gassed with an atmosphere of 95% air-5% $CO_2$.

Sodium arsenite was prepared as a 1 mM stock solution in saline A (8.182 g/l NaCl, 0.372 g/l KCl, 0.336 g/l $NaHCO_3$, and 0.9 g/l glucose, pH 7.4) and stored at 4°C. Cells ($1.5 \times 10^5$ cells/ml) were exposed to arsenite, and/or other addictions, in the respective complete culture medium, as detailed in the text, as well as in the legends to the figures.

**2.4 DHR and MitoSOX red fluorescence assay.** The cells were supplemented with either 10 μM DHR or 5 μM MitoSOX red for 30 min and subsequently exposed for the last 10 min to arsenite. In other experiments, cells were exposed for increasing time intervals to arsenite and DHR was added to the culture medium in the last 30 min of incubation. After the treatments, the cells were washed 3 times with saline A and fluorescence images were captured with a BX-51 microscope (Olympus, Milan, Italy) equipped with a SPOT-RT camera unit (Diagnostic Instruments, Delta Sistemi, Rome, Italy) using an Olympus LCAch 40x/0.55 objective lens. The excitation and emission wavelengths were 488 and 515 nm (DHR) and 510 and 580 nm (MitoSOX red), with a 5-nm slit width for both emission and excitation. Images were collected with exposure times of 100–400 milliseconds, digitally acquired and processed for fluorescence determination at the single-cell level on a personal computer using ImageJ software. Mean fluorescence values were determined by averaging the fluorescence values of at least 50 cells per treatment condition per experiment.

**2.5 Measurement of intracellular free calcium levels and mitochondrial $Ca^{2+}$.** Cells were treated for 30 min with either 4 μM Fluo-4 or 10 μM Rhod 2-AM and subsequently exposed for the last 10 min to arsenite. After the treatments, the cells were washed 3 times with saline A and subsequently analyzed with a fluorescence microscope. The resulting images were taken and processed as described above. The excitation and emission wavelengths were 488 and 515 nm (Fluo-4) and 540 and 590 nm (Rhod 2-AM), with a 5-nm slit width for both emission and excitation. Images were collected with exposure times of 100–400 ms, digitally acquired and processed for fluorescence determination at the single-cell level on a personal computer using the ImageJ software. Mean fluorescence values were determined by

averaging the fluorescence values of at least 50 cells per treatment condition per experiment.

**2.6 Super resolution and confocal microscopy.** U-U937 and D-C2C12 cells were grown in arsenite for 6 h and Rhod 2-AM together with MitoTracker Deep Red tracker were added to the culture medium in the last 30 min. Confocal and Structured Illumination microscopy (SIM) was done on a Nikon SIM system with a 100x 1.49 NA oil immersion objective, managed by NIS elements software. Raw and reconstructed images were validated with the SIM check plugin of Image. Four different fields were randomly selected throughout the wells and imaged at laser excitation of 561 nm (Rhod-2AM) and 640 nm (mitochondria with MitoTracker Deep Red) with a 3D-SIM acquisition protocol. Confocal images were quantified with ImageJ. Colocalisation between Rhod 2-AM and MitoTracker was analyzed using the Jacop ImageJ plugin and expressed as Manders index.

**2.7 Immunofluorescence analysis.** HeLa, U-U937, D-U937, U-C2C12 or D-C2C12 cells were grown in 35 mm tissue culture dishes containing an uncoated coverslip, incubated for 16 h in the absence or presence of arsenite. After the treatment, the U-U937 or D-U937 cells were centrifuged, incubated for 10 min in 2 ml of saline A to allow cells to attach to the coverslip. Then, cells were fixed for 1 min with 95% ethanol/5% acetic acid, washed with phosphate buffer saline (PBS, 136 mM NaCl, 10 mM $Na_2HPO_4$, 1.5 mM $KH_2PO_4$, 3 mM KCl; pH 7.4) and blocked in PBS-containing bovine serum albumin (2% w/v) (30 min at room temperature). The cells were subsequently incubated with the primary antibody (1:100 in PBS containing 2% bovine serum albumin), stored for 18 h at 4°C, washed and then incubated for 3 h in the dark with fluorescein isothiocyanate-conjugated secondary antibody diluted 1:100 in PBS. The cells were then analyzed with a fluorescence microscope to count the relative numbers of cells bearing a punctate fluorescence, consistent with mitochondrial localization of

cytochrome c, and a diffused fluorescence, consistent with the mitochondrial loss of cytochrome c. In each experiment, at least 150 cells were analyzed to calculate the percentage of cells with a diffused fluorescence, indicative of MPT-dependent loss of cytochrome c.

**2.8 Western Blot analysis.** Cells were plated in 60 mm or 100 mm dishes. When cells reached 80% confluence, cell culture medium was discarded and dishes were washed 2 times in PBS; then, the lysis buffer (10 mM Tris-HCl pH 7.4, 10 mM $MgCl_2$, 100 mM NaCl and 0.1% Triton) was added. The lysate was collected in Eppendorf tubes and centrifuged at 14000 rpm for 5 min at 4 °C. The supernatant was used for electrophoresis and the pellet was discarded. Laemmli Sample Buffer 1× (0.125 M Tris HCl pH 6.8, 10% SDS, 20% glycerol, 1 M DTT, 0.004% bromophenol blue) was added to protein extracts and then the extracts were loaded into a polyacrylamide gel (Stacking gel: 5% Bis-acrylamide, 0.3 M Tris-HCl pH 6.8, 5% SDS, 1% ammonium persulfate, 0.2% TEMED; Running gel: 12% Bis-acrylamide, 0.3 M Tris-HCl pH 8.8, 0.5 M SDS, 1% ammonium persulfate, 0.25 % TEMED). Electrophoresis was performed in 1× running buffer (3.03 g Tris Base, 14.4 g glycine, 0.1% SDS) at 25 mA for 1 h. Proteins were transferred from the gel to a nitrocellulose membrane (Wet/Tank Blotting System, Bio-Rad) using transfer buffer with 20% of methanol at 100 V for 1 h. To block non-specific sites, the membrane was incubated with 5% bovine serum albumin or milk (Bovine Serum Albumin, Sigma) in TBS (0.1 M Tris-HCl pH 7.4, 0.8 M NaCl). The membrane was incubated in primary antibodies diluted in 5% milk in TBST (TBS and 0.1% Tween) for 1 h at room temperature or overnight at 4°C. After 3 washes in TBST, the membrane was probed with horseradish peroxidase-conjugated anti-rabbit or anti-mouse IgG antibodies at room temperature for 1 h and visualized with enhanced chemiluminescence (ECL). Band intensity was quantified by densitometry using ImageJ and normalized to loading controls.

For non-reducing SDS-PAGE, cells were treated with 20 mM NEM to quench free thiols.

**2.9 Redox Western Blot analysis.** The Trx2 redox state was estimated by redox western blots as described in (Folda et al., 2016). Briefly, after treatments, the cells (2.5 x $10^6$) were washed with PBS (136 mM NaCl, 10 mM $Na_2HPO_4$, 1.5 mM $KH_2PO_4$, 3 mM KCl; pH 7.4) and resuspended in 150 µl of urea lysis buffer (100 mM Tris/HCl, pH 8.2; 8 M urea; 1 mM EDTA) containing 10 mM iodoacetoamide. The samples were then incubated for 20 min at 37°C and centrifuged at 14,000g for 1 min. Ten volumes of cold acetone/1 M HCl (98:2) were added to the supernatants, and the pellets were washed twice with acetone/1 M HCl/$H_2O$ (98:2:10). The pellets were resuspended in 60 µl of urea lysis buffer containing 3.5 mM dithiothreitol and, after a 30 min incubation at 37 °C, supplemented with 30 mM iodoacetoamide and incubated for a further 30 min at 37 °C. Samples were then subjected to urea-PAGE (7 M urea and 7% acrylamide) under non-reducing conditions and blotted (Folda et al., 2016).

**2.10 Fluorogenic Caspase 3 assay.** Caspase 3–like activity was monitored as described in (Guidarelli et al. 2005). Briefly, the cells were lysed and aliquots of the extract (30 µg proteins) were incubated with 12 µM of Acetyl-Asp-Glu-Val-Asp-7-amido-4-methylcoumarin, at 30 °C. Caspase 3–like activity was determined fluorometrically (excitation at 360 nm and emission at 460 nm) by quantifying the release ofaminomethylcoumarin from cleaved caspase 3 substrate at appropriate intervals.

**2.11 Analysis of apoptosis with Hoechst 33342 assay.** After treatments, the cells were incubated for 5 min in the presence of 10 µM Hoechst 33342 and then analyzed with a fluorescence microscope to assess their nuclear morphology (chromatin condensation and fragmentation). Cells with homogeneously stained nuclei were considered viable.

**2.12 Cytotoxicity assay.** After treatments with arsenite, the number of viable cells was estimated with the trypan blue exclusion assay. Briefly, an aliquot of the cell suspension was diluted 1:2 (v/v) with 0.4% trypan blue and the viable cells (*i.e.*, those excluding trypan blue) were counted with a hemocytometer.

**2.13 Alkaline Halo assay.** DNA single-strand breakage was determined using the alkaline halo assay that was developed in our laboratory (Cantoni and Guidarelli, 2008). It is important to note that, although we refer to DNA strand scission throughout the text, the DNA nicks measured by this technique under alkaline conditions may in fact include alkali labile sites in addition to direct strand breaks. Details on the alkaline halo assay, processing of fluorescence images and the calculation of the experimental results are also given in ref. (Cantoni and Guidarelli, 2008). DNA single-strand breakage was quantified by calculating the nuclear spreading factor value, representing the ratio between the area of the halo (obtained by subtracting the area of the nucleus from the total area, nucleus + halo) and that of the nucleus, from 50 to 75 randomly selected cells/experiment/treatment condition.

**2.14 ATP determination.** Ice-cold 5% perchloric acid was added to the cells ($2 \times 10^6$ cells). After a 10 min incubation in an ice bath, the samples were centrifuged for 5 min at 10,000 g. The supernatants were neutralized with 3 M $K_2CO_3$ and the precipitates were removed by centrifugation. Ten percent (v/v) 1 M $KH_2PO_4$ (pH 6.5) was added to the nucleotide-containing supernatants. The samples were then filtered through 0.22-μm pore microfilters. The clear filtered solutions were directly analyzed by high-performance liquid chromatography (HPLC) with the UV detection wavelength set at 254 nm (Stocchi et al., 1985). The liquid chromatographic system used consisted of a System Gold Programmable Solvent Module 125 and a System Gold Programmable Solvent Detector 166 (Beckman,

Fullerton, CA). The HPLC separation was performed using a 5-µm Supelco Discovery C18 column (15 cm x 4.6 mm) equipped with a 5-µm Supelguard Discovery 18 (2 cm x 4.0 mm) (Supelco, Bellefonte, PA). The mobile phase used for the separation consisted of buffer A (0.1 M $KH_2PO_4$) and buffer B (90:10 buffer A/methanol). The following gradient of buffer B was used: 25% in 9 min, 90% in 6 min, and 100% in 2.5 min. Buffer B (100%) was held for 2 min, and 100%–0% was reached in 6 min. Re-equilibration with buffer A for 5 min was performed before each injection. The injected volume was 20 µl, and the flow rate was 1.3 ml/min.

**2.15 Measurement of GSH content by High-Performance Liquid Chromatography.** The cells (1 x $10^6$) were suspended in 100 µl of lysis buffer, vortexed and kept for 10 min on an ice bath. Thereafter, 15 µl of 0.1 N HCl and 140 µl of precipitating solution (0.2 M glacial meta-Phosphoric acid, 5 mM sodium EDTA, 5 M NaCl) were added to the samples. After centrifugation, the supernatants were collected and kept at 220°C until the HPLC analyses. Just before analysis, 60 µl of the acid extract was supplemented with 15 µl of 0.3 M $Na_2HPO_4$ and 15 µl of a solution containing 20 mg of 5,5'- dithiobis (2-nitrobenzoic acid) in 100 ml of sodium citrate (1% w/v). The mixture was stirred for 1 min at room temperature and, after 5 min, filtered through 0.22-µm pore microfilters. The clear filtered solution was directly analyzed by HPLC, with the UV detection wavelength set at 330 nm for their glutathione (GSH) content (Brundu et al., 2016), using a 15 cm x 4.6 mm, 5-mm Supelco Discovery C18 column (Supelco, Bellefonte, PA). The UV absorption was detected at 330 nm. The injection volume was 20 ml. The retention time of GSH was approximately 15.7 min. The liquid chromatographic system used is the same described in the previous paragraph (ATP determination). The HPLC separation was performed using a 15 cm x 4.6 mm, 5-µm Supelco Discovery C18 column equipped with a 5-µm Supelguard Discovery 18 (2 cm x 4.0 mm). The

mobile phase used for the separation consisted of buffer A (0.1 M $KH_2PO_4$) and buffer B (40:60 buffer A/acetonitrile). The following gradient of buffer B was used: 0%–100% in 15 min; 100% buffer B was held for 5 min, and 100%–0% was reached in 20 min. Re-equilibration with buffer A for 10 min was performed before each injection. The injected volume was 20 µl, and the flow rate was 1 ml/min.

**2.16 Real-time quantitative RT-PCR analysis.** Total RNA was isolated using the RNeasy mini-Kit (Qiagen) following the manufacturer's instructions. One microgram of total RNA was reverse-transcribed and analyzed using the Applied Biosystems' real-time PCR System and the ΔΔCt method. Relative gene expression in cells was normalized to cyclophilin mRNA levels.

The sequence of primer pairs is:

hs-ATF4_Fw GGT TCT CCA GCG ACA AGG_Rv TCT CCA ACA TCC AAT CTG TCC

hs-CHOP_Fw CAT CAC CAC ACC TGA AAG CA_Rv TCA GCT GCC ATC TCT GCA

hs-CYCLOPHILIN_Fw GAC CCA ACA CAA ATG GTT CC_Rv TTT CAC TTT GCC AAA CAC CA.

**2.17 Statistical analysis.** The results are expressed as means ± S.D. Statistical differences were analyzed by one-way ANOVA followed by Dunnett's test for multiple comparison or two-way ANOVA followed by Bonferroni's test for multiple comparison using Prism 6.0 software (GraphPad Software). We used an unpaired *t*-test for two group analyses. A value of $P < 0.05$ was considered significant.

# 3. Results and Discussion

## 3.1 Arsenite-induced mitochondrial superoxide formation: time and concentration requirements for the effects of the metalloid on the endoplasmic reticulum and mitochondria

In our previous studies (Fiorani et al., 2018), we found that exposure of U-U937 cells to 2.5 μM arsenite causes a time-dependent DHR fluorescence response, barely appreciable at 3 h and progressively more significant at 6 and 16 h. We recapitulated these experiments and found that the time-dependence is lost after addition of ATP (100 μM), an $IP_3R$ agonist (Berridge, 1993), or Cf (10 mM), a RyR agonist (Meissner, 2017), in the last 10 min of arsenite exposure (Fig. 1A). More specifically, we observed similar responses in cells treated for 16 h with arsenite, or for only 0.5 h with the metalloid and ATP or Cf supplementation in the final 10 min. In other experiments performed in cells loaded with DHR prior to treatment with arsenite, we obtained a maximal response under conditions of 10 min co-exposure to the metalloid and ATP, or Cf (Fig. 1B).

Next, we investigated the arsenite concentration dependence using the same 10 min co-exposure protocol. As indicated in Fig. 1C, ROS formation was already maximal at 0.5 μM arsenite and significant at concentrations as low as 100 nM.

Collectively, the experimental results thus far discussed indicate that ATP or Cf supplementation promotes maximal ROS formation after a very short exposure to very low concentrations of arsenite.

In the above experiments, ROS formation was detected using DHR, a fluorescence probe that allows detection of $H_2O_2$ and other ROS as $O_2^{-\cdot}$, $OH^{\cdot}$ or peroxinitrite. It is however important to note that, as indicated by our previous studies (Guidarelli et al, 2015, 2016), the slow DHR-fluorescence response induced by arsenite is entirely mediated by species generated *via* a

$Ca^{2+}$-dependent mechanism at the level of mitochondria, *i.e.*, mito$O_2^{\cdot-}$, which dismutates to diffusible $H_2O_2$, causing deleterious effects in mitochondrial and extra-mitochondrial compartment.

We therefore investigated whether the DHR fluorescence response induced by arsenite/ATP or /Cf was mediated by the same mechanism or by others (*e.g.*, NADPH oxidase).

We found that the DHR fluorescence response induced by arsenite/Cf, while insensitive to the $IP_3R$ antagonist 2-APB (Maruyama et al., 1997), was prevented by Ry, a RyR antagonist (Meissner, 2017), as well as by the MCU inhibitor Ru360 (Zazueta et al., 1999). These results suggest that ROS formation is mediated by a mechanism in which the fraction of $Ca^{2+}$ released from the RyR is cleared by the mitochondria. To support further this notion, we investigated the effects of Cf, alone or associated with arsenite, on $Ca^{2+}$ homeostasis.

Cf (10 min) increased both the $[Ca^{2+}]_c$ (Fig. 1E) and the $[Ca^{2+}]_m$ (Fig. 1F) and these responses were abolished by Ry and unaffected by 2-APB. Ru360 selectively abolished the increase in the $[Ca^{2+}]_m$, with hardly any effect detected on the $[Ca^{2+}]_c$. Identical responses were obtained using Cf associated with arsenite, which failed to promote detectable effects in the absence of the RyR agonist.

We then demonstrated that the DHR fluorescence response induced by arsenite/ATP was suppressed by 2-APB, Ry as well as Ru360 (Fig. 1D). Thus, as observed with arsenite/Cf, ROS formation appears mediated by a mechanism in which the fraction of $Ca^{2+}$ released from the RyR is associated with the mitochondrial accumulation of the cation.

Consistently, ATP caused a significant increase in $[Ca^{2+}]_c$ (Fig. 1E) and $[Ca^{2+}]_m$ (Fig. 1F), once again unaffected by arsenite. These responses were abolished by 2-APB. Ry and Ru360 suppressed mitochondrial $Ca^{2+}$ accumulation with respectively very little or no effect on the $[Ca^{2+}]_c$.

These results are therefore consistent with the notion that the mechanism whereby $IP_3R$ and RyR agonists enhance ROS formation induced by a 10-min exposure to arsenite involves enforced mitochondrial $Ca^{2+}$ accumulation.

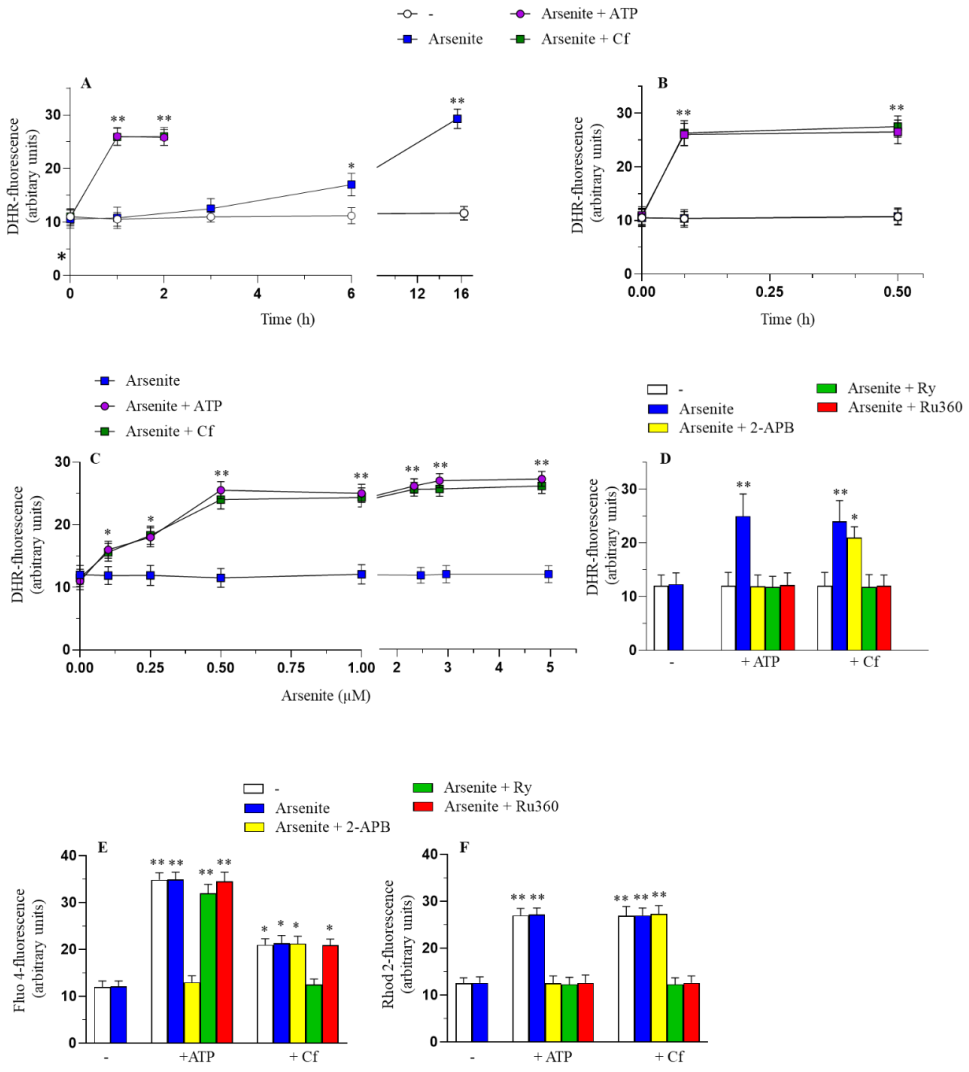


Guidarelli et al., J Pharmacol Exp Ther, 2020

**Fig. 1. Time- and concentration-dependence for the arsenite-induced ROS formation in the absence or presence of $Ca^{2+}$ mobilizing agents.** (A) U-U937 cells were exposed for increasing time intervals to 2.5 μM arsenite, supplemented in the last 30 and 10 min of incubation with DHR and ATP (100 μM) or Cf (10 mM), respectively, and finally analyzed for the resulting DHR fluorescence responses. (B) Cells were preloaded with DHR (30 min), treated for 10 or 30 min with arsenite and exposed to ATP or Cf in the last 10 min of incubation. (C) Cells were preloaded with DHR (30 min) and then exposed for 10 min to ATP or Cf with or without increasing concentrations of arsenite. (D) Cells preloaded with DHR (30 min) were exposed for 5 min to the vehicle, 2-APB (50 μM), Ry (20 μM) or Ru360 (10 μM) and finally treated for a further 10 min with 2.5 μM arsenite with or without ATP or Cf. After treatments, the cells were analyzed for their DHR fluorescence. (E-F) Cells pre-loaded for 30 min with Fluo-4-AM (E), or Rhod-2-

AM (F), were exposed for 5 min to 2-APB, Ry or Ru360 and treated for a further 10 min with 2.5 µM arsenite, with or without ATP or Cf. Cells were then analyzed for their fluorescence responses. Results represent the means ± S.D. calculated from at least three separate experiments. *P<0.05; **P<0.01, as compared with untreated cells. (A-C) Two-way ANOVA followed by Bonferroni's test; (D,E,F) one-way ANOVA followed by Dunnet's test.

We next investigated whether the above events were indeed associated with mito$O_2^{-\cdot}$ formation and eventually if there was also a role for NADPH oxidase activation. The initial experiments showed that the DHR fluorescence response induced by arsenite in combination with either Cf or ATP is sensitive to rotenone (an inhibitor of complex I) or L-ascorbic-acid (AA) (Fig 2A). Rotenone and AA instead failed to affect the $[Ca^{2+}]_m$ elicited by Cf, or ATP, in combination with the metalloid (Fig. 2B). Importantly, AA was used under conditions promoting a significant accumulation of the vitamin in mitochondria, thereby causing an effective scavenging of mitochondrial ROS (Fiorani et al., 2018).

Experiments performed using MitoSOX red, a fluorochrome commonly employed for the detection of $O_2^{-\cdot}$ in the mitochondria of live cells, confirmed the mitochondrial origin of the ROS.

These results therefore indicate that most, if not all, the ROS produced using the co-exposure protocol are generated in the mitochondrial respiratory chain. Consistently, experiments performed in respiration-deficient U937 (RD-U937) cells demonstrated a lack of ROS formation (using both DHR and MitoSOX red) after treatment with arsenite/ATP or /Cf, despite the observed increases in $[Ca^{2+}]_m$, remarkably similar to those found in U-U937 cells.

As expected, there was no evidence of NADPH oxidase activation after a 10 min exposure to arsenite associated with ATP (Fig. 2D and E) or Cf (not shown). More specifically, we found that the DHR-fluorescence response induced by PMA was sensitive to apocynin and DPI (two NADPH oxidase inhibitors), with hardly effect mediated by these inhibitors on the DHR fluorescence response induced by arsenite/ATP. Moreover PMA, unlike

arsenite/ATP, promoted an apocynin- or DPI-sensitive p47$^{phox}$ phosphorylation (Fig. 2E).

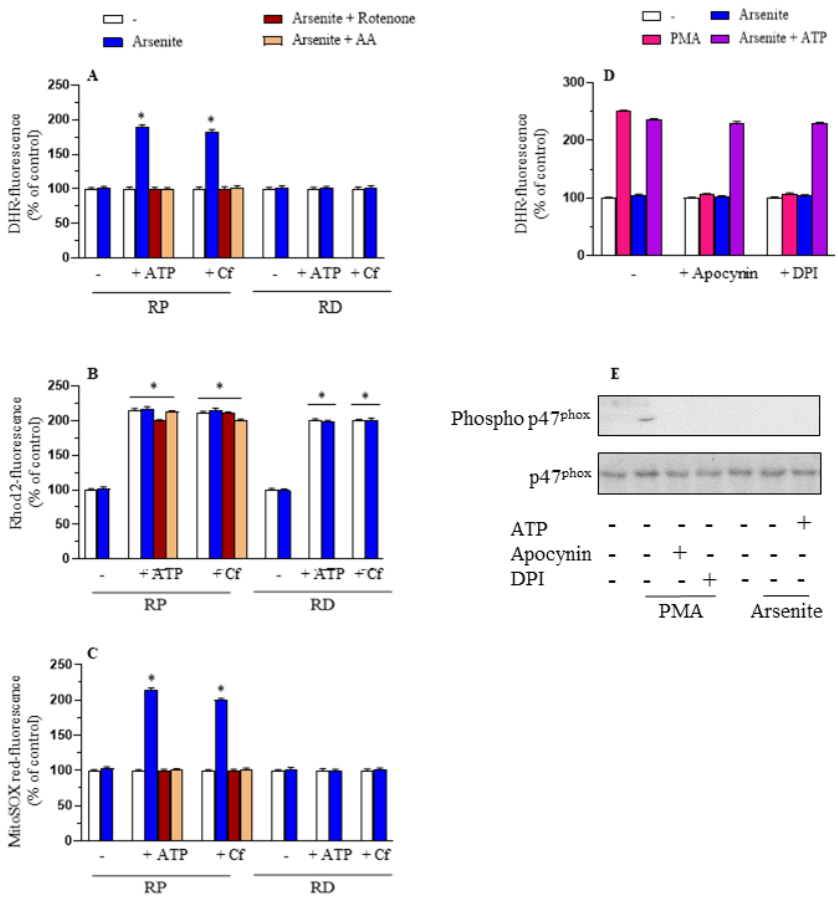


Guidarelli et al., J Pharmacol Exp Ther, 2020

**Fig. 2**. **ROS formation induced by short-term co-exposure to low concentrations of arsenite and the $Ca^{2+}$ mobilizing agents takes place in the mitochondrial respiratory chain.** (A–C) U-U937 and RD-U937 cells (RP- and RD-cells) pre-loaded for 30 min with DHR (A), Rhod-2-AM (B), or MitoSOX red (C) were exposed for 5 min to the vehicle, rotenone (0.5 μM), or AA (10 μM) and were finally treated for a further 10 min with 2.5 μM arsenite with or without ATP or Cf. After treatments, the cells were analyzed for the resulting fluorescence responses. (D) U-U937 cells pre-loaded with DHR (30 min), were exposed for 5 min to the vehicle, apocynin (10 μM) or DPI (1 μM) and for a further 10 min to the arsenite alone or associated with ATP. In some experiments, the cells were exposed for 30 min to PMA (100 ng/ml) in the absence or presence of apocynin or DPI. After treatments, the cells were analysed for DHR-fluorescence. (E) The cells treated as indicated in D were analyzed for phospho p47$^{phox}$ expression. The blot, representative of three separate experiments, was re-probed for p47$^{phox}$. Results represent the means ± S.D. calculated from at least three separate experiments. *P < 0.01, as compared to untreated cells (one-way ANOVA followed by Dunnet's test).

Thus, the short-term exposure to arsenite/ATP or /Cf, as previously observed after prolonged exposure to the metalloid alone, leads to the exclusive

formation of mito$O_2^{-\cdot}$. Since this process is $Ca^{2+}$-dependent, the dramatic effects mediated by ATP or Cf are likely attributable to their ability to rapidly promote mitochondrial $Ca^{2+}$ accumulation. In this perspective, the slow ROS response induced by arsenite alone was dependent on events associated with $Ca^{2+}$ mobilization from the ER and the subsequent increased $[Ca^{2+}]_m$.

We finally investigated whether mito$O_2^{-\cdot}$ formation induced by arsenite/ATP or /Cf was associated with the onset of toxic events. There was no evidence for a decline in GSH and ATP levels, instead, readily observed using $H_2O_2$ as a positive control (not shown). We also performed Redox Western blots and did not obtain evidence of thioredoxin 2 (Trx2) oxidation in mitochondria. This event was instead readily detected using increasing concentrations of diamide (Fig. 3), as expected from other studies (Stanley et al., 2011; Folda et al., 2016).

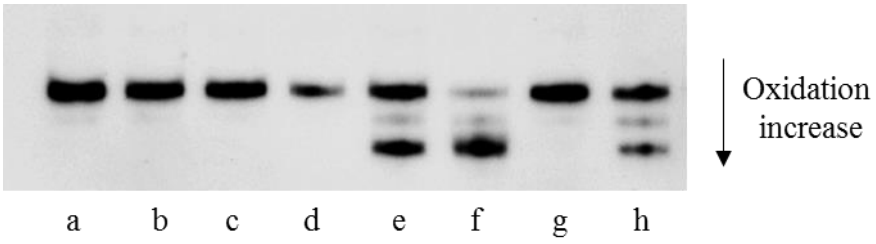


Guidarelli et al., J Pharmacol Exp Ther, 2020

**Fig. 3 Short-term exposure to arsenite/ATP or Cf did not change the redox state of Trx2.** U-U937 cells ($2.5 \times 10^6$), treated for 10 min as detailed below, were processed for the analysis of reduced, partially oxidized and fully oxidized Trx2 thiol groups. The redox state of Trx2 was measured by urea-PAGE under non-reducing conditions. (a) control; (b) 2.5 μM arsenite; (c) arsenite and ATP (d) arsenite and Cf (e), 0.5 mM diamide (60 min), (f) 1 mM diamide (60 min), (g) control, (h) mobility standard.

In other experiments, the cells were treated for 10 min with 2.5 μM arsenite alone, or associated with ATP or Cf, and then analyzed after 0, 6 and 48 h of growth in drug-free medium. Under these different conditions, we did not observe caspase 3 activation (Fig. 4A), chromatin

condensation/fragmentation (Fig. 4B), or reduced cell proliferation rates (Fig. 4C). Instead, evidence documenting caspase 3 activation (Fig. 4A), DNA fragmentation (Fig. 4B) and a significant reduction in the counts of viable cells (Fig. 4C) was obtained in cells exposed for 48 h to arsenite.

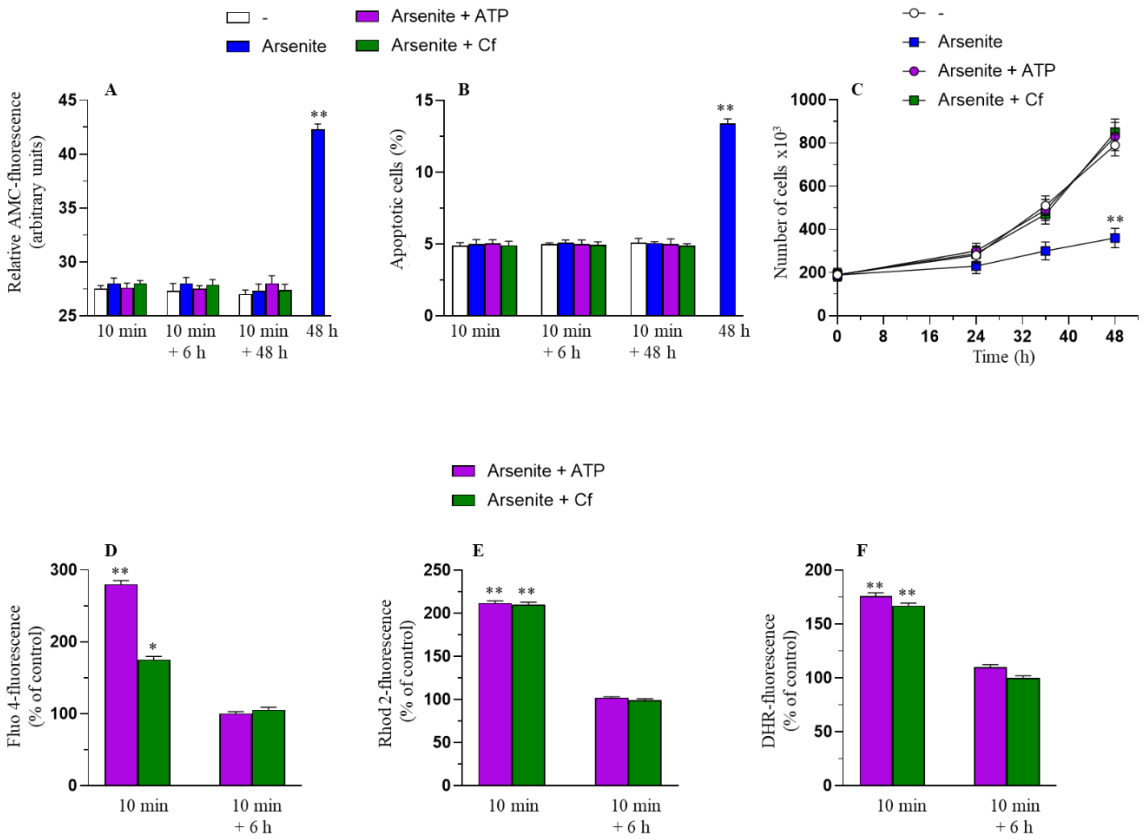


Guidarelli et al., J Pharmacol Exp Ther, 2020

**Fig. 4. MitoO$_2^{\cdot-}$ generated by the short-term co-exposure to arsenite and ATP or Cf fail to induce toxicity.** (A and B) U-U937 cells exposed for 10 min to 2.5 μM arsenite with or without ATP or Cf and analyzed for their caspase 3 activity (A) or for apoptosis, detected by measuring chromatin fragmentation/condensation (B), either immediately or after 6 or 48 h of growth in fresh culture medium. In other experiments, the cells were grown for 48 h in the presence of arsenite (A and B). (C) Cells were treated as indicated above and finally counted after growth in fresh culture medium for increasing time intervals. The closed circles indicate cells grown in the continuous presence of arsenite. (D–F) Cells were loaded (30 min) with Fluo 4-AM (D), Rhod-2-AM (E), or DHR (F) and then treated for 10 min as indicated in the figure. After treatments, the cells were processed to determine the respective fluorescence responses either immediately or 6 h post-incubation in fresh culture medium. Results represent the means ± S.D. calculated from at least three separate experiments. *P < 0.05; **P < 0.01, as compared with untreated cells. (A, B, and D–F) One-way ANOVA followed by Dunnet's test; (C) two-way ANOVA followed by Bonferroni's test.

The lack of toxic consequences in the short-term co-exposure protocol is probably due to the reversibility of the upstream effects mediating ROS formation. This notion is clearly established by the results of experiments showing that the initial effects observed at 10 min on the $[Ca^{2+}]_c$ (Fig. 4D), $[Ca^{2+}]_m$ (Fig. 4E) and DHR-fluorescence response (Fig. 4F) return to control levels even after 6 h of post-treatments incubation.

In the next set of experiments, cells exposed to arsenite/ATP or /Cf were processed with the alkaline halo assay to determine DNA strand scission. The results shown in Fig. 5A indicate that cells exposed to any of the following agents, arsenite (30 min), ATP (10 min) or Cf (10 min), do not present signs of DNA damage. Ethidium bromide-stained cells that received these treatments were indeed identical to controls. Fig. 5A also provide typical images of cells with damaged DNA, as in cells receiving a 6 h exposure to arsenite, characterized by increased halo/reduced nuclear remnants. It was then interesting to observe that the DNA damaging response was even more pronounced in cells exposed for 30 min to arsenite with ATP or Cf supplemented in the last 10 min.

We analyzed the time dependence of DNA strand scission in cells exposed for increasing time intervals to arsenite, with or without ATP, or Cf, in the last 10 min of incubation. When cells were treated only with arsenite, the nuclear spreading factor increased very slowly (Fig. 5B), in contrast to treatments with the metalloid and ATP, or Cf, in which the accumulation of DNA lesions was extremely faster (Fig. 5A). We also showed that, using the same co-exposure protocol, maximal DNA-damaging responses were induced by 0.5-1 µM arsenite (Fig. 5C).

Finally, we demonstrated that the effects induced by 1 µM arsenite associated with ATP and Cf were abolished by treatments preventing ROS formation at the level of mitochondrial respiratory chain (rotenone or the respiration-deficient phenotype), or through their scavenging (AA), or by

preventing mitochondrial $Ca^{2+}$ accumulation (Ry, Ru360). The $IP_3R$ antagonist 2-APB prevented the DNA strand scission induced by arsenite/ATP.

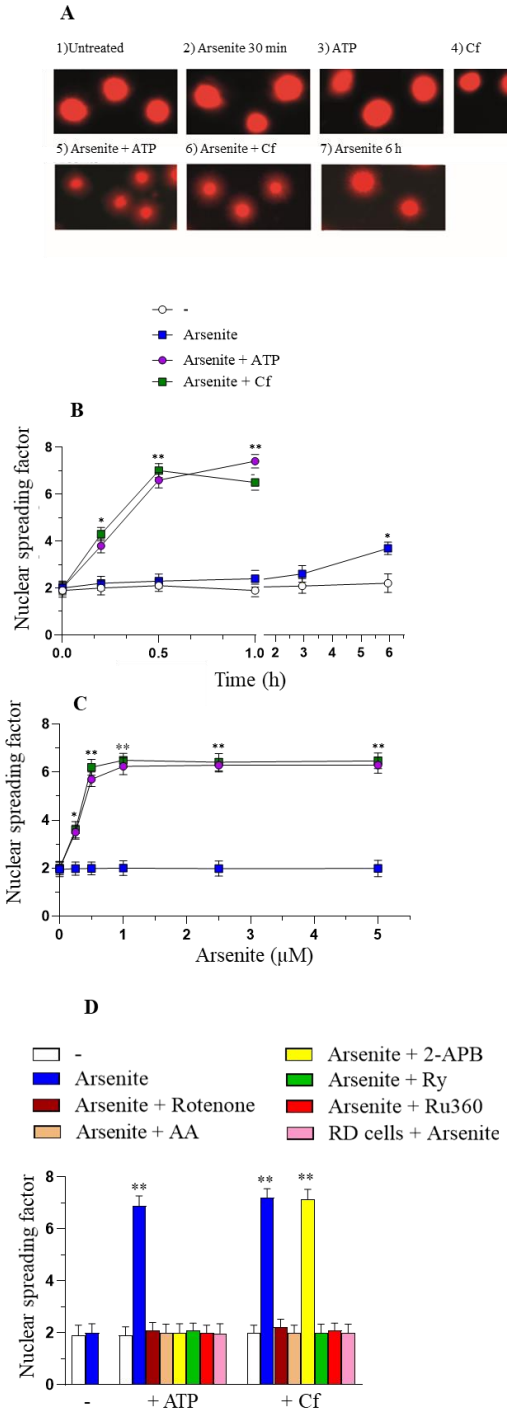


Guidarelli et al., J Pharmacol Exp Ther, 2020

**Fig. 5. Mito$O_2^{-\cdot}$ generated by the short-term coexposure to arsenite and ATP or Cf lead to DNA single-strand breakage.** (A) Representative micrographs of U-U937 cells treated for 30 min with the vehicle (A 1), 2.5 µM arsenite

(A 2), ATP (in the last 10 min, A 3), Cf (in the last 10 min, A 4), arsenite and ATP (A 5) or arsenite and Cf (A 6) and finally processed with the alkaline halo assay. (A 7) Micrograph of cells exposed for 6 h to arsenite. (B) U-U937 cells exposed for increasing time intervals to 2.5 μM arsenite received a 10 min treatment with ATP or Cf at the end of the incubation and were subsequently analyzed for DNA damage by the alkaline halo assay. (C) Cells exposed for 30 min to increasing concentrations of arsenite received ATP or Cf in the last 10 min and were then immediately analyzed for DNA damage. (D) U-U937 cells were exposed for 5 min to the vehicle, rotenone, AA, 2-APB-, Ry or Ru360 for a further 30 min to 2.5 μM arsenite with or without ATP or Cf in the last 10 min of incubation and finally analyzed for DNA strand scission. In some experiments, the DNA-damaging response was measured in RD-U937 cells (RD cells) co-exposed for 30 min to arsenite and ATP or Cf. Results represent the means ± S.D. calculated from at least three separate experiments (B and C) Two-way ANOVA followed by Bonferroni's test; (D) one-way ANOVA followed by Dunnet's test.

The results presented in this section indicate that the prolonged exposure to arsenite resulting in mito$O_2^{-\cdot}$ formation is necessary to affect $Ca^{2+}$ homeostasis and accumulate the cation in mitochondria. The arsenite time and concentration requirements to promote mito$O_2^{-\cdot}$ formation in the presence of sufficient mitochondrial $Ca^{2+}$ were instead remarkably lower. Finally, the short-term exposure to arsenite/ ATP or /Cf associated with $Ca^{2+}$-dependent mito$O_2^{-\cdot}$ formation, on the one hand failed to promote toxicity and the other hand effectively promoted DNA single strand breakage.

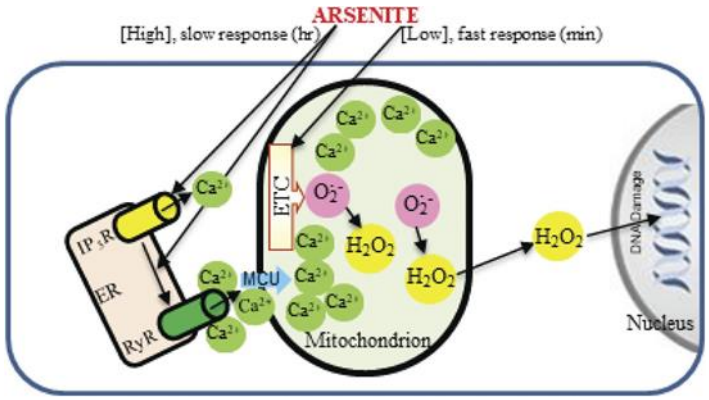


Guidarelli et al., J Pharmacol Exp Ther, 2020

**Fig. 6. Arsenite requirements for maximal $Ca^{2+}$-dependent mito$O_2^{-\cdot}$/$H_2O_2$ formation.** Prolonged (h) exposure to high concentrations of arsenite is necessary to target the $IP_3R$ and the crosstalk between this pool and the RyR to

promote RyR-derived $Ca^{2+}$ accumulation in mitochondria. These events are favored by the specific architecture of the ER and by the close apposition between the RyR and mitochondria of U-U937 cells. Remarkably shorter exposure to significantly lower concentrations of the metalloid are instead required to maximally generate mito$O_2^{-\cdot}$ under optimal conditions of $Ca^{2+}$ availability. This notion was clearly established by enforcing mitochondrial $Ca^{2+}$ accumulation with $IP_3R$ or RyR agonists, and the resulting mito$O_2^{-\cdot}$ and its dismutation product, $H_2O_2$, although failing to promote mitochondrial dysfunction and MPT-dependent apoptosis, nevertheless caused extensive DNA strand scission.

### 3.2 Functional organization of the endoplasmic reticulum dictates the susceptibility of target cells to arsenite-induced mitochondrial superoxide formation, mitochondrial dysfunction and apoptosis

Based on the results presented in the previous section, it appears that mito$O_2^{-\cdot}$ formation induced by arsenite can only occur under conditions in which the mitochondrial accumulation of $Ca^{2+}$ is enhanced after the initial stimulation of the $IP_3R$ and the successive recruitment of the RyR. In U-U937 cells, this second channel is in close apposition with mitochondria and the fraction of the cation derived from the $IP_3R$ is not directly cleared by these organelles. Given this premise, we may expect that the arsenite-induced mitochondrial $Ca^{2+}$ accumulation and ROS formation are restricted to cell types expressing both the $IP_3R$ and RyR.

We therefore performed a comparative study using various cell lines, including U-U937 cells. These cells, which as previously mentioned express both $IP_3R$ and RyR (Sugiyama et al., 1994; Clementi et al., 1998; Hosoi et al., 2001; Guidarelli et al. 2009), can be differentiated to monocyte-like cells (D-U937 cells), with a concomitant loss of RyR expression (Guidarelli et al., 2009). We also used undifferentiated C2C12 (U-C2C12) cells that instead gained RyR expression after differentiation (D-C2C12 cells). U-C2C12 cells therefore uniquely expressed the $IP_3R$, in contrast to D-C2C12 cells, which expressed both channels. Finally, we used HeLa cells, which express only the $IP_3R$.

Consistently with this premise, we found that a 10 min exposure to 10 mM Cf fails to increase the $[Ca^{2+}]_c$ in HeLa, D-U937 and U-C2C12 cells (Fig. 7A). A significant $Ca^{2+}$ response, sensitive to Ry and insensitive to 2-APB, was instead obtained in U-U937 and D-C2C12 cells. ATP promoted a significant increase in $[Ca^{2+}]_c$, sensitive to 2-APB, in all cell types (Fig. 7B). Ry failed to affect the $Ca^{2+}$ response induced by ATP in HeLa, U-C2C12 and

D-U937 cells, with a minor inhibitory effect induced in U-U937 and D-C2C12 cells.

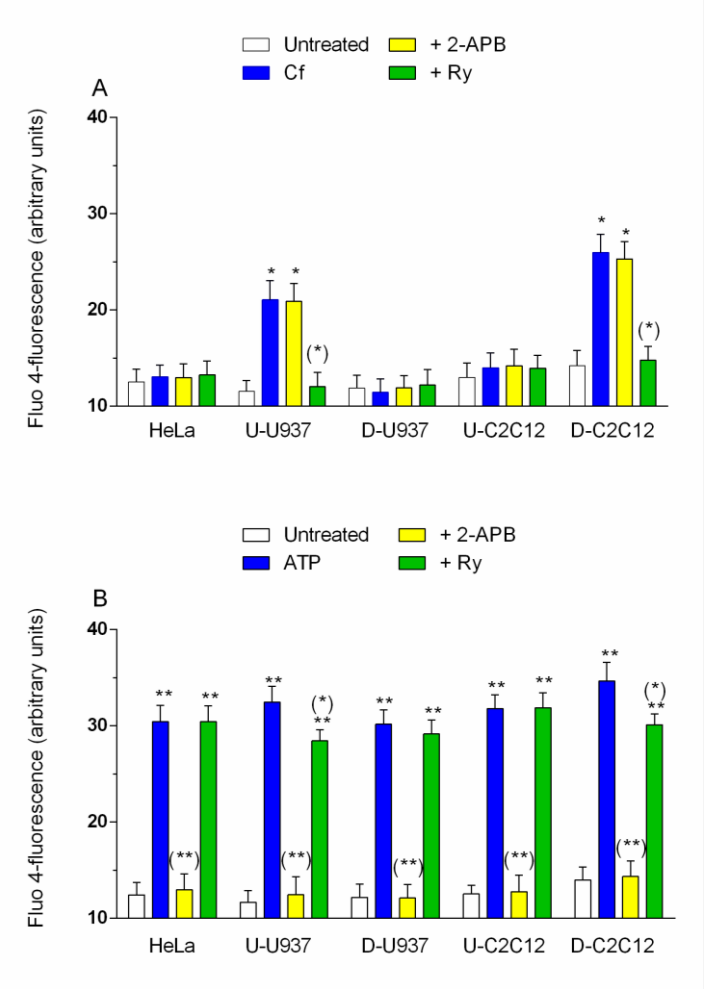


Guidarelli et al., Food and Chemical Toxicology, 2021

**Fig. 7. Characterization of the $Ca^{2+}$ responses mediated by $IP_3R$ and RyR agonists in HeLa, U-U937, D-U937, U-C2C2 and D-C2C12 cells.** Cells were pre-exposed for 20 min to Fluo 4-AM and then treater for 10 min with 10 mM Cf (A) or 100 µM ATP (B). In some experiments, 2-APB or Ry was added to the cultures 5 min prior to Cf or ATP. After treatments, the cells were analyzed for Fluo 4-fluorescence. The results represent the means ± S.D. calculated from at least three distinct experiments. *P <0.05, **P <0.01, as compared to untreated cells. (*) $P < 0.05$, (**) $P < 0.01$, as compared to cells treated with agonists (ANOVA followed by Dunnett's test).

Thus, we provide functional evidence documenting the notion that HeLa, U-C2C12 and D-U937 cells, unlike U-U937 and D-C2C12 cells, do not express the RyR. $IP_3Rs$ were instead expressed in all cell types employed in our experiments.

We also performed toxicity studies and found that a 6 h exposure to 2.5 µM arsenite fails to promote toxic effects in all the above cell types, as assessed by the trypan blue exclusion assay (which detects loss of plasma membrane integrity) (Fig. 8A) or the Hoechst assay (which detects apoptotic DNA fragmentation and condensation) (Fig. 8B).

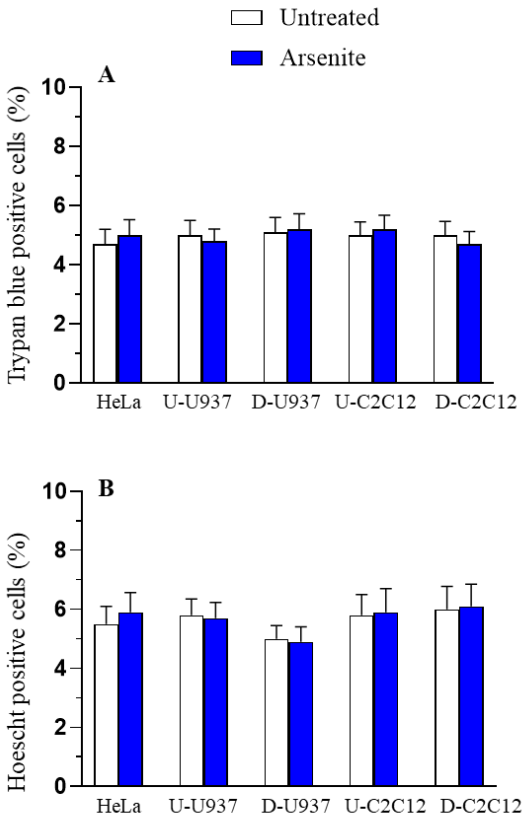


Guidarelli et al., Food and Chemical Toxicology, 2021

**Fig. 8. The 6 h arsenite exposure paradigm fails to promote detectable signs of toxicity in different cell lines.** HeLa, U-U937, D-U937, U-C2C12 and D-C2C12 were exposed for 6 h to 2.5 µM arsenite and then counted with a hemocytometer in the presence of trypan blue (A). Under identical conditions, the cells were also analyzed for chromatin fragmentation/condensation (B). The results represent the means ± S.D. calculated from at least three distinct experiments.

Next, we analyzed the $Ca^{2+}$ response induced by the metalloid and obtained evidence for a limited increase in $[Ca^{2+}]_c$ in HeLa, U-C2C12 and D-U937 cells, sensitive to 2-APB and not affected by Ry (Fig. 9A). Different results were instead obtained in cells expressing both the $IP_3R$ and the RyR, in which the $Ca^{2+}$ response was remarkably greater, abolished by 2-APB and significantly reduced by Ry. It is interesting to note that the fraction of $Ca^{2+}$ released by U-U937 and D-C2C12 cells treated with arsenite and Ry was similar to that released by D-U937, U-C2C12 and HeLa cells exposed to arsenite alone.

We then tested the effect of increasing concentrations of arsenite and found that the resulting $Ca^{2+}$ response was mediated by a saturable mechanism in cells expressing only the $IP_3R$, with a maximal increase in $[Ca^{2+}]_c$ being observed at 2.5 µM. U-U937 and D-C2C12 cells showed a concentration-dependent increase in $[Ca^{2+}]_c$ after exposure to 2.5-10 µM arsenite (Fig. 9B). Interestingly, the $Ca^{2+}$ responses mediated by arsenite in the presence of Ry in U-U937 and in D-C2C12 were similar to those mediated by the metalloid alone in HeLa, D-U937 and U-C2C12 cells.

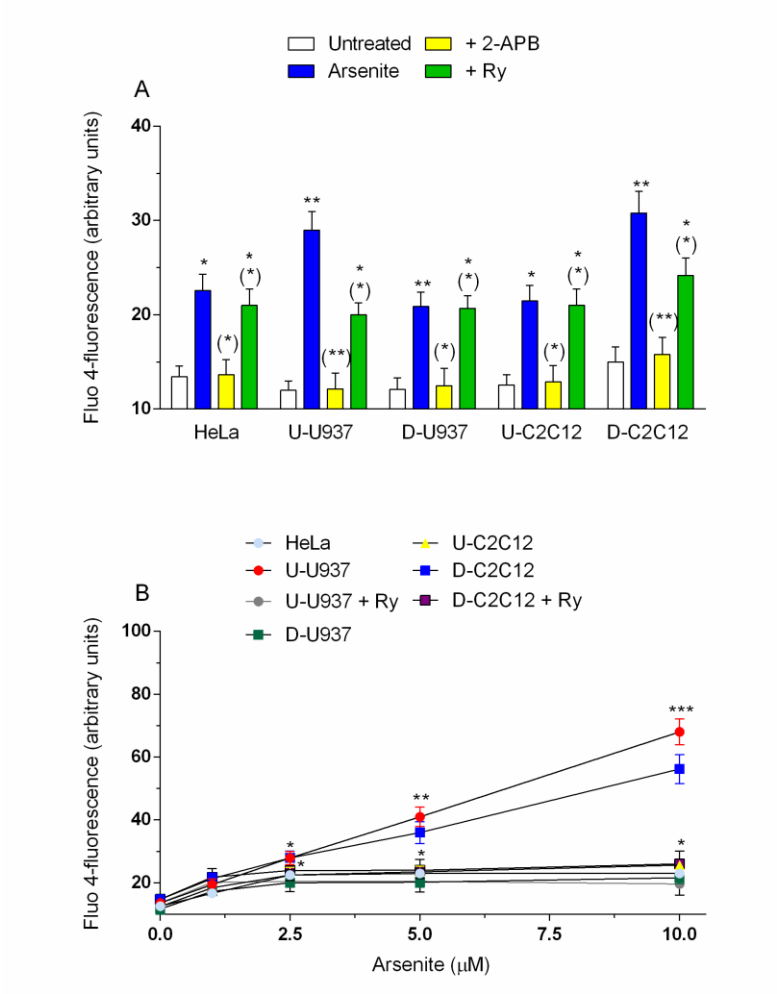


Guidarelli et al., Food and Chemical Toxicology, 2021

**Fig. 9**. **Arsenite induces different $Ca^{2+}$ responses in cells expressing the $IP_3R$, with or without concomitant RyR expression.** (A) Cells were pre-exposed for 5 min to the vehicle, 2-APB or Ry and subsequently incubated for 6 h in the presence of 2.5 μM arsenite. After treatments, the cells were analyzed for Fluo 4-fluorescence. The results represent the means ± S.D. calculated from at least three distinct experiments. *P <0.05, **P <0.01, as compared to untreated cells. (*) $P < 0.05$, (**) $P < 0.01$, as compared to cells treated with arsenite (ANOVA followed by Dunnett's test). (B) Cells were exposed for 6 h to increasing concentrations of arsenite and finally analyzed for Fluo 4-fluorescence. The effect of Ry was tested in U-U937 and D-C2C12 cells. The results represent the means ± S.D. calculated from at least three distinct experiments. *P <0.05, **P <0.01, ***P <0.001, as compared to untreated cells (two-way ANOVA followed by Bonferroni's test).

In the next series of experiments, we investigated whether ATP promotes mitochondrial $Ca^{2+}$ accumulation in the above cell types. We found that the $IP_3R$ agonist significantly increased the $[Ca^{2+}]_m$ in HeLa, D-U937 and U-C2C12 cells *via* a mechanism sensitive to Ru360 and 2-APB but insensitive to Ry. ATP increased the $[Ca^{2+}]_m$ also in U-U937 and D-C2C12 cells,

however *via* a mechanism that, besides being sensitive to 2-APB and Ru360, was abolished also by Ry.

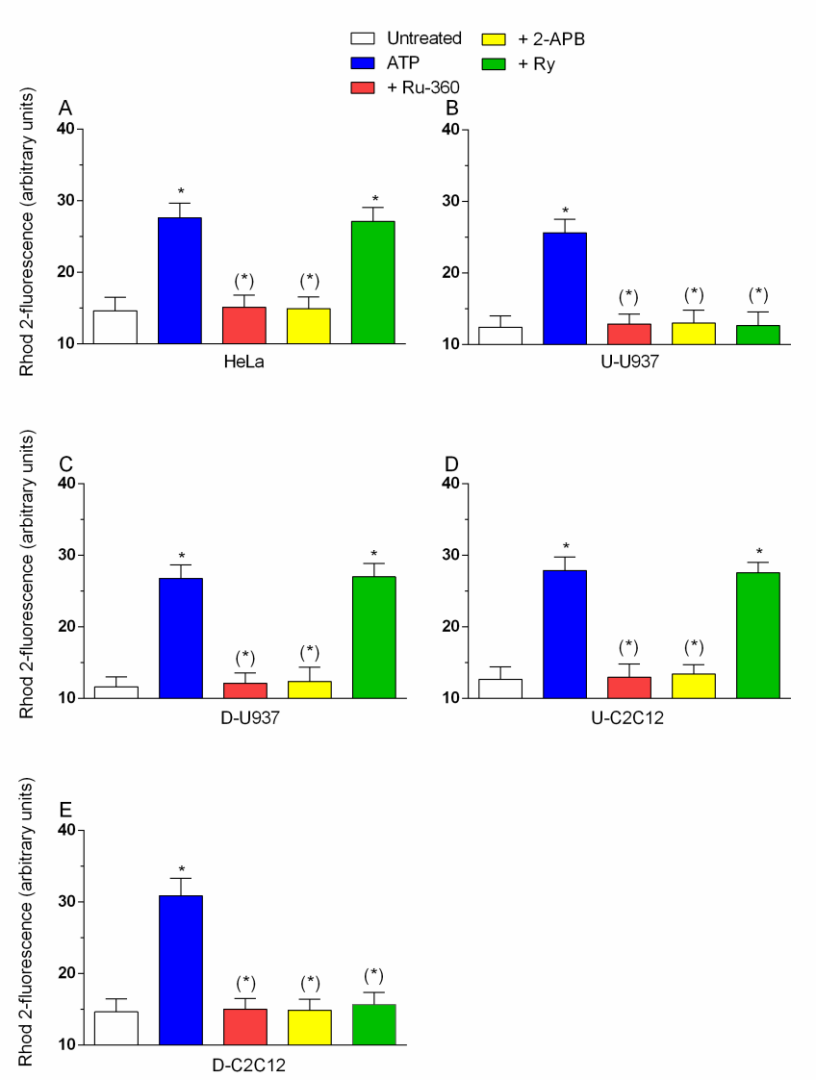


Guidarelli et al., Food and Chemical Toxicology, 2021

**Fig. 10. ATP stimulation increases the mitochondrial accumulation of $Ca^{2+}$ in cells expressing the $IP_3R$, with or without concomitant RyR expression.** HeLa (A), U-U937 (B), D-U937 (C), U-C2C12 (D) and D-C2C12 (E) cells were pre-exposed for 5 min to the vehicle, Ru-360, 2-APB or Ry and treated for a further 10 min with 100 µM ATP. After treatments, the cells were analyzed for Rhod 2-fluorescence. The results represent the means ± S.D. calculated from at least three distinct experiments. *P <0.01, as compared to untreated cells. (*) P < 0.01, as compared to cells treated with ATP (ANOVA followed by Dunnett's test).

Thus, ATP directly promotes mitochondrial $Ca^{2+}$ accumulation in cells that do not express the RyR, thereby demonstrating that in these cells the $IP_3R$ and mitochondria are in close apposition. In RyR expressing cells, the $IP_3$

releasing agonist instead caused mitochondrial $Ca^{2+}$ accumulation with the intermediate involvement of the RyR.

Exposure to arsenite (2.5 µM for 6 h) promoted mitochondrial $Ca^{2+}$ accumulation only in cells expressing the RyR (Fig. 11A-F) and these responses were sensitive to Ru360, 2-APB and Ry (panels B and E). There was no evidence of mitochondrial $Ca^{2+}$ accumulation in HeLa, D-U937 and U-C2C12 even using greater arsenite concentrations (Fig. 11F). The metalloid instead caused a concentration-dependent mitochondrial uptake of $Ca^{2+}$ in U-U937 and D-C2C12 (Fig. 11F). The increase of mitochondrial $Ca^{2+}$ was also confirmed by confocal and SIM microscopy in D-C2C12 (Fig. 11G).

The above results there indicate that ATP -but not arsenite- promotes mitochondrial $Ca^{2+}$ accumulation in cells expressing only the $IP_3R$. Both ATP and arsenite increased $[Ca^{2+}]_m$ in cells expressing both channels and for this purpose the recruitment of the RyR after the initial stimulation of the $IP_3R$ appears critical.

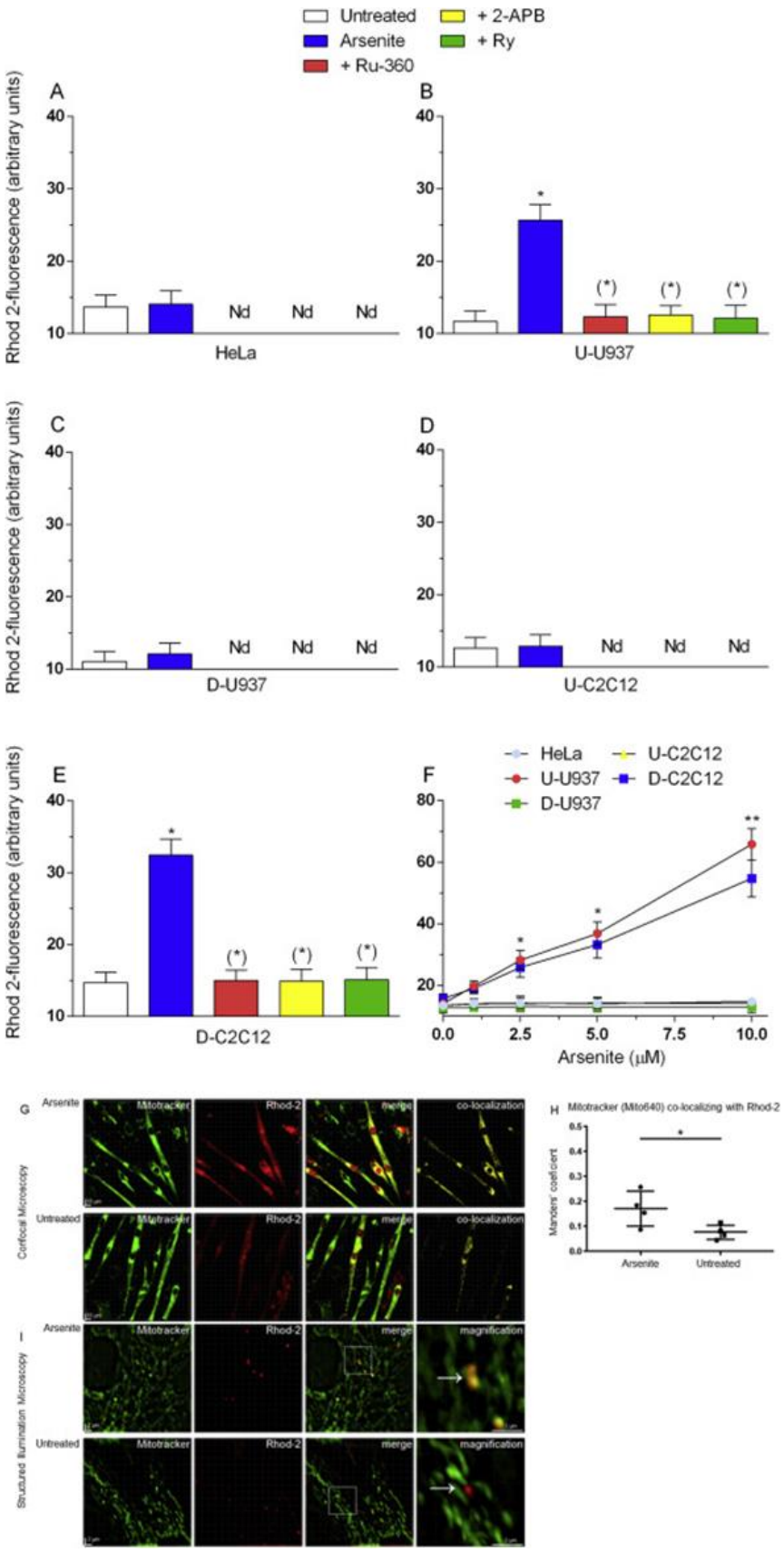


Guidarelli et al., Food and Chemical Toxicology, 2021

**Fig. 11. Arsenite fails to increase the mitochondrial concentration of $Ca^{2+}$ in cells uniquely expressing the $IP_3R$.** HeLa (A), U-U937 (B), D-U937 (C), U-C2C12 (D) and D-C2C12 (E) cells were pre-exposed for 5 min to the vehicle, Ru-360, 2-APB or Ry and incubated for a further 6 h in the presence of 2.5 µM arsenite. After treatments, the cells were analyzed for Rhod 2-fluorescence. The results represent the means ± S.D. calculated from at least three distinct experiments. *P <0.01, as compared to untreated cells. (*) P < 0.01, as compared to cells treated with arsenite (ANOVA followed by Dunnett's test). (F) Cells were incubated with increasing concentrations of arsenite for 6 h. After treatments, the cells were analyzed for Rhod 2-fluorescence. The results represent the means ± S.D. calculated from at least three distinct experiments. (N.d., not detectable). *P <0.01, **P <0.001, as compared to untreated cells (two-way ANOVA followed by Bonferroni's test). (G) D-C2C12 cells were incubated for 6 h with or without 2.5 µM arsenite. After treatments, the cells were analysed to determine the co-localization of Rhod 2-AM (green) and MitoTracker Deep Red (red) fluorescence signals. On the right, panels display the merged image of the two stains. (H) Manders coefficient of Rhod 2-fluorescence in mitochondria was calculated as the proportion of Rhod 2-fluorescence signal overlapping with the signal of the Mitotracker in four randomly acquired fields. The results represent the means ± S.D. (*) P <0.05 as compared to untreated cells (Two-tailed unpaired *t* test). (I) High Resolution SIM images of Mitotracker signal (green) and Rhod 2-AM (red) in D-C2C12 cells. Inserts represent area where Rhod 2-AM signal colocalizes with that of the Mitotracker in arsenite-treated D-C2C12.

Next, we analyzed ROS formation using both DHR and MitoSOX red after a 6 h exposure to 2.5 µM arsenite. The results illustrated in Fig. 12 indicated that the metalloid fails to promote ROS formation in HeLa, D-U937 and U-C2C12 cells. Both fluorescence responses were instead detected in U-U937 and D-C2C12 cells and were in both circumstances sensitive to 2-APB, Ry and Ru-360.

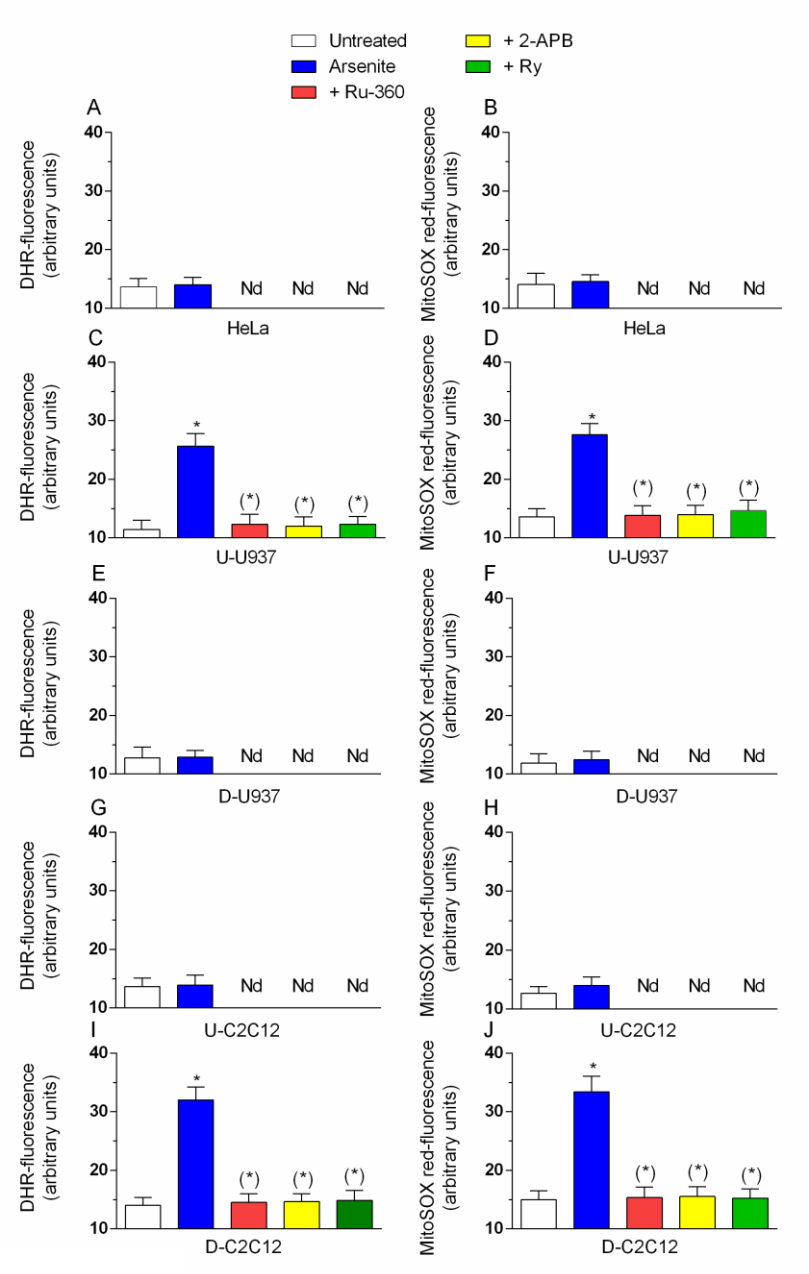


Guidarelli et al., Food and Chemical Toxicology, 2021

**Fig. 12. Arsenite fails to induce mito$O_2^{\cdot-}$ formation in cells with only $IP_3R$.** HeLa (A, B), U-U937 (C, D), D-U937 (E, F), U-C2C12 (G, H) and D-C2C12 (I, J) cells were pretreated for 5 min with the vehicle, Ru-360, 2-APB or Ry and incubated for 6 h with the further addition of 2.5 μM arsenite. After treatments, the cells were analyzed for DHR- (A,C,E,G,I) or MitoSOX red (B,D,F,H,J) -fluorescence. The results represent the means ± S.D. calculated from at least three distinct experiments. (N.d., not detectable). *P <0.01, as compared to untreated cells. (*) P < 0.01, as compared to cells treated with arsenite (ANOVA followed by Dunnett's test).

These results therefore provide convincing evidence that arsenite uniquely promotes mito$O_2^{-\cdot}$ formation in responsive RyR-expressing cells. Although from the above data it appears clear that the resistance of HeLa, D-U937 and U-C2C12 to mito$O_2^{-\cdot}$ formation induced by arsenite is uniquely due to the lack of mitochondrial $Ca^{2+}$ accumulation, we nevertheless decided to provide a further proof of evidence. We reasoned that the resistance of these cells should be lost under conditions in which the mitochondrial accumulation of the cation is enforced by other treatments, as ATP. HeLa, D-U937 or U-C2C12 cells were therefore exposed for 6 h to arsenite and ATP was added in the final 10 min. Under these conditions, arsenite promoted a significant MitoSOX red fluorescence response in the three cell types, sensitive to 2-APB and Ru-360 and insensitive to Ry (Fig. 13).

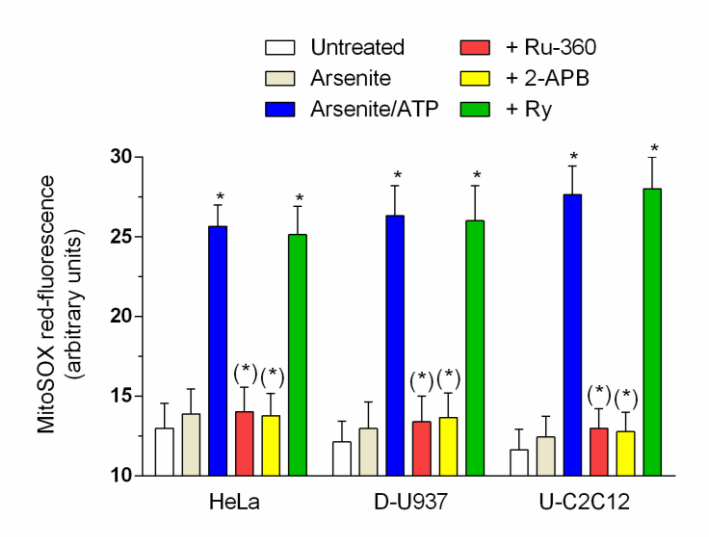


Guidarelli et al., Food and Chemical Toxicology, 2021

**Fig. 13. ATP promotes mito$O_2^{-\cdot}$ formation in response to arsenite in cells uniquely expressing the $IP_3R$.** HeLa, D-U937 and U-C2C12 cells were incubated for 6 h with 2.5 µM arsenite, rinsed and resuspended in fresh culture medium containing the vehicle, Ru360, 2-APB or Ry. After 5 min, cells received 100 µM ATP for a further 10 min and were finally analyzed for MitoSOX red fluorescence. The results represent the means ± S.D. calculated from at least three distinct experiments. *P <0.01, as compared to untreated cells. (*) P <0.01, as compared to cells treated with arsenite/ATP (ANOVA followed by Dunnett's test).

These results therefore provide conclusive evidence supporting the notion that arsenite fails to promote mito$O_2^{\cdot -}$ formation in cells uniquely expressing the $IP_3R$ for the only reason that RyR expression is strictly required to increase the $[Ca^{2+}]_m$.

We finally performed toxicity studies and observed that a 16 h exposure to arsenite causes a decline in mitochondrial membrane potential (Fig. 14 Bi and Ei) and mitochondrial loss of cytochrome c (Fig. 14 Bii and Eii) only in RyR expressing cells. In the same cells, these events were followed by caspase 3 activation (Fig. 14 Biii and Eiii), decreased MTT conversion to formazan (Fig. B iv and E iv), reduced U937 cells proliferation (Fig. 1 Bv; D-C2C12 are differentiated, non-proliferating cells) and apoptotic fragmentation (Fig. 14 Bvi and Evi) at 24 h. There was no evidence for changes in the above parameters in cells uniquely expressing the $IP_3R$ (Fig. 14 A,C,D).

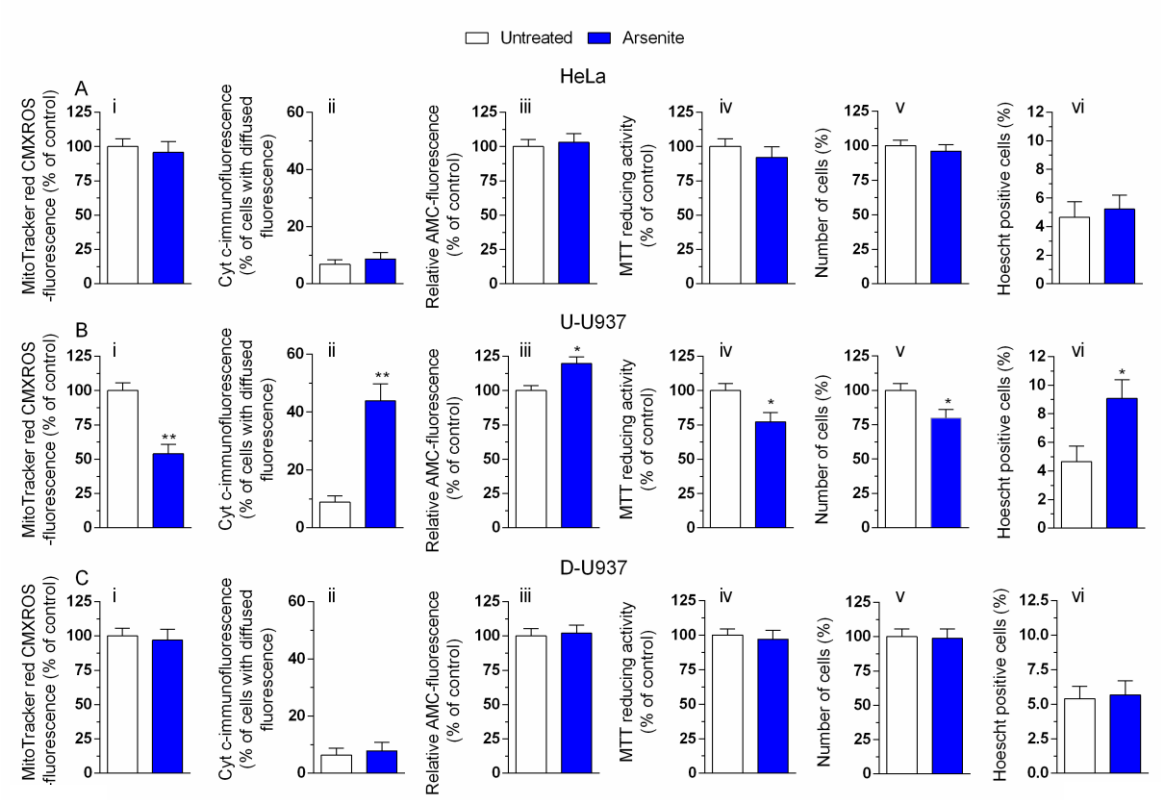

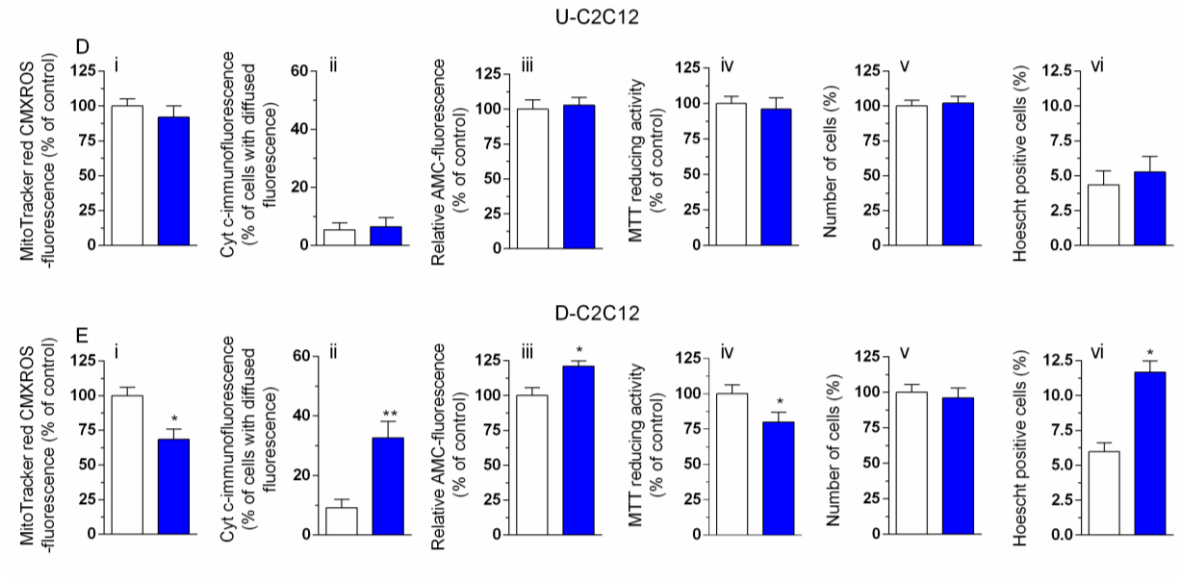


Guidarelli et al., Food and Chemical Toxicology, 2021

**Fig. 14. Arsenite causes mitochondrial dysfunction and apoptosis in cells with both $IP_3R$ and RyR.** HeLa (A), U-U937 (B), D-U937 (C), U-C2C12 (D) and D-C2C12 (E) cells were treated for 16 (A-Eiii) or 24 h (a-eiii-vi) with arsenite. After treatments, the cells were analyzed for MitoTracker red CMXRos-fluorescence (A-Ei), cytochrome c localization (A-Eii), caspase 3 activity (A-Eiii), MTT reducing activity (A-Eiv) and toxicity by either quantifying the number of viable cells (A-Ev) or measuring chromatin fragmentation/condensation (A-Evi). The results represent the means ± S.D. calculated from at least three distinct experiments. *P <0.01, *P <0.001 as compared to untreated cells (ANOVA followed by Dunnett's test).

### 3.3 ERO1α mediates recruitment of the ryanodine receptor after inositol 1, 4, 5-trisphosphate receptor stimulation induced by arsenite

The above studies indicate that RyR expression and recruitment are critical for the triggering of events leading to arsenite-induced mito$O_2^{\cdot -}$ formation. We therefore decided to investigate the mechanism of RyR recruitment and for this purpose initially investigated whether arsenite causes an ER stress, under the same conditions associated with mito$O_2^{\cdot -}$ formation. We found that a 6 h treatment of U-U937 cells with 2.5 μM arsenite causes a significantly increase in ATF4 (Fig. 15A) and CHOP (Fig. 15B) mRNA levels and a nearly threefold increase in ERO1α protein expression (Fig. 15C). These results indicate that arsenite is an effective ER stress inducer (Sun, 2017) in the conditions employed in our experiments. We also provide evidence for an increased expression of the CHOP target, ERO1α, an ER oxidoreductase potentially mediating RyR recruitment after arsenite stimulation.

In order to address this issue, we decided to employ the inhibitor EN460, which interacts with the reduced form of ERO1α thereby blunting its oxidase activity. As indicated in Fig. 15, in untreated U-U937 cells, ERO1α is in a reduced form. Indeed, ERO1α showed a similar mobility on a non-reducing SDS-PAGE in samples with or without DTT (lanes 1 and 2, Fig. 15D). Addition of EN460 (10-50 μM), promoted the accumulation of a higher molecular weight disulfide-bonded ERO1α form associated with the loss of the faster migrating bands. Thus, even at the lowest concentration tested, EN460 affects the redox state of ERO1α, thereby inhibiting its oxidase activity. Importantly, there was no evidence of toxicity (as determined by the Hoechst and trypan blue assays) under the conditions employed in our experiments (6 h incubation) in cells exposed to EN460 alone or associated with arsenite.

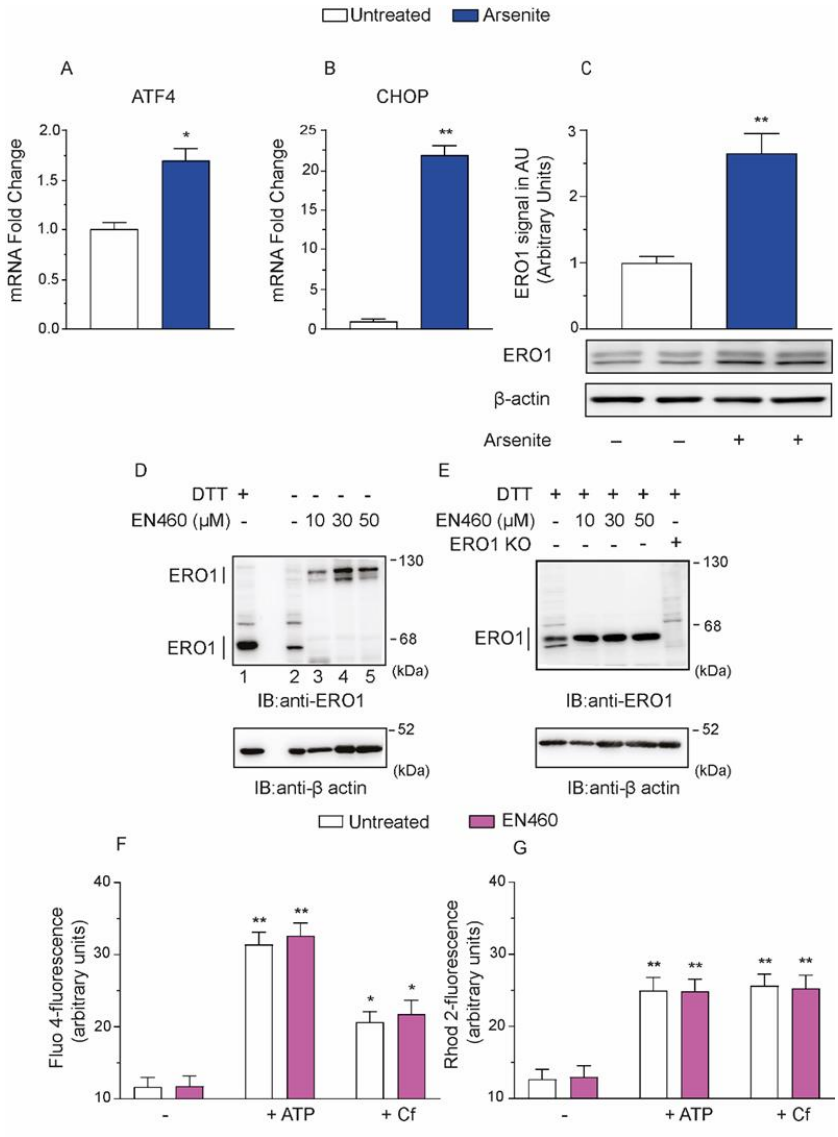


Unpublished data

**Fig. 15. Arsenite induces ER stress and ERO1α expression.** U-U937 cells were exposed for 6 h to 2.5 μM arsenite and subsequently processed to determine ATF4 (A) or CHOP (B) mRNA expression, as well as ERO1α (C) protein expression. Anti-β-actin antibody was used as a loading control. Cells were incubated for 6 h in the absence or presence of 10, 30 or 50 μM EN460. Cells were then washed and lysed in the presence of 20 mM NEM, and proteins were resolved on a non-reducing SDS-PAGE (D, the lanes between 1 and 2 is empty) or in a reducing SDS-PAGE after adding 100 mM DTT to the sample buffer (E). Anti-β-actin antibody was used as a loading control. In other experiments, cells were exposed for 6 h to 10 μM EN460, washed, re-suspended in fresh culture medium, loaded (20 min) with Fluo 4 (F), or Rhod 2 (G), and subsequently incubated for 10 min with 100 μM ATP or 10 mM Cf. After treatments, the cells were analyzed for their respective fluorescence responses. Results represent the means ± S.D. calculated from at three separate experiments. *P <0.05; **P <0.01 compared with untreated cells (ANOVA followed by Dunnett's test).

We then analyzed the effects of the inhibitor on $Ca^{2+}$ homeostasis after stimulation (10 min) with ATP, or Cf, and found that EN460 fails to affect

the increases in the $[Ca^{2+}]_c$ (Fig. 15F) and $[Ca^{2+}]_m$ (Fig. 15G) mediated by both agonists.

As previously discussed, in U-U937 cells arsenite induces an increase in $[Ca^{2+}]_c$ abolished by 2-APB and partially reduced by Ry (Fig. 16A). EN460 induced an effect remarkably similar to that mediated by Ry. In D-U937 cells, devoid of a functional RyR, arsenite caused a limited increase in $[Ca^{2+}]_c$ (Fig. 16B), abolished by 2-APB, but insensitive to either Ry or EN460 (Fig. 16B). In U-U937 cells, arsenite also promoted an increase in $[Ca^{2+}]_m$ sensitive to 2-APB, Ry as well as EN460 (Fig. 16C). Under identical conditions, arsenite failed to promote mitochondrial $Ca^{2+}$ uptake in D-U937 cells (Fig. 16D).

Interestingly, arsenite induced a MitoSOX red fluorescence response abolished by all treatments, including EN460, preventing mitochondrial $Ca^{2+}$ accumulation. In addition, there was no evidence of mito$O_2^{-\cdot}$ formation in D-U937 cells (Fig. 16F).

We next analyzed the effects of agents preventing $Ca^{2+}$ mobilization and/or its mitochondrial accumulation induced by arsenite on ERO1α expression. The results illustrated in Fig. 16G indicate that ERO1α expression was suppressed by 2-APB and partially reduced by Ry. In D-U937 cells, we obtained only a limited increase in ERO1α expression, suppressed by 2-APB and insensitive to Ry (Fig. 16H).

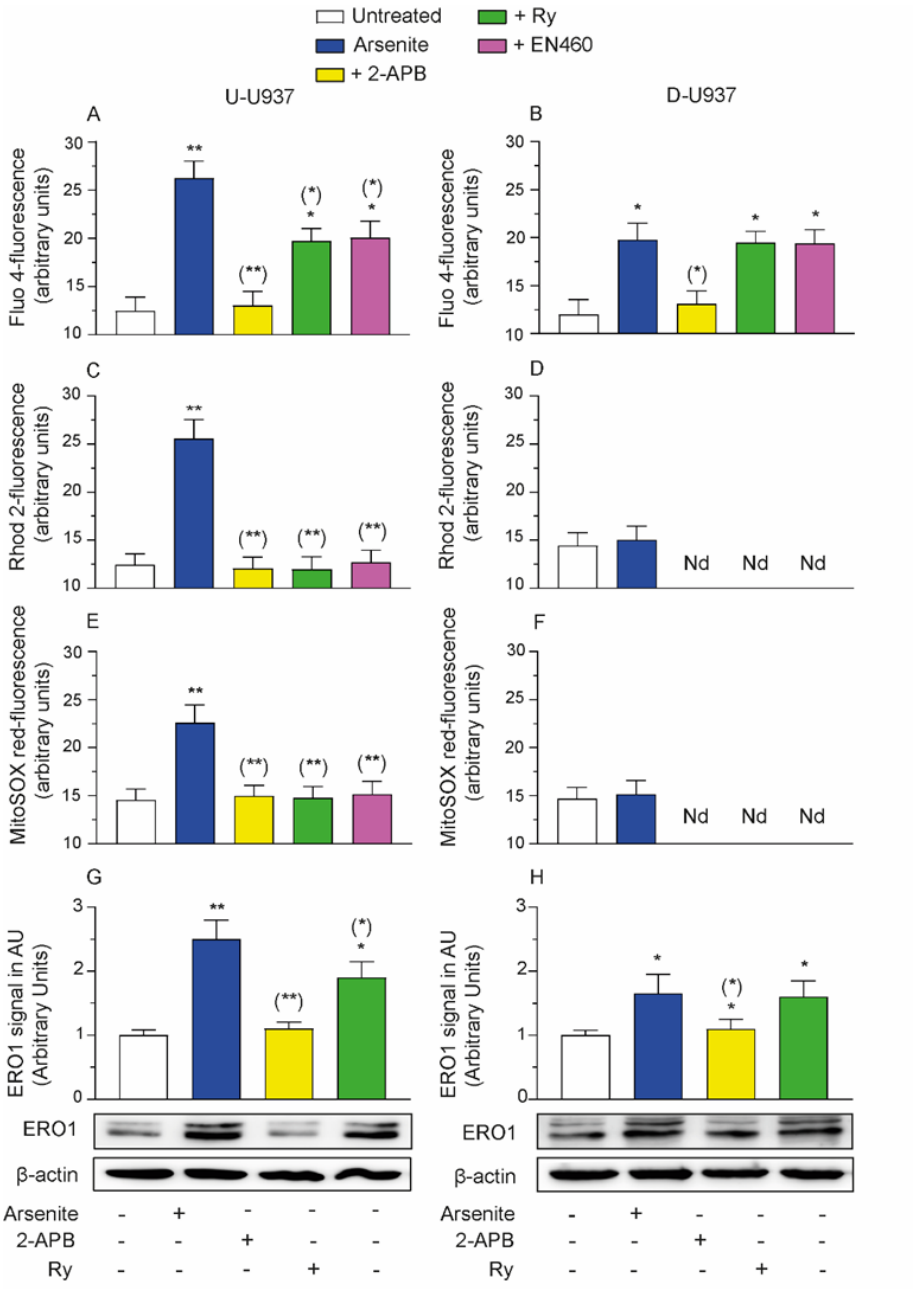


Unpublished data

**Fig. 16. Arsenite-induced stimulation of $Ca^{2+}$ release from the $IP_3R$ mediates ERO1α enhanced expression, in turn responsible for the recruitment of the RyR, critical for mitochondrial $Ca^{2+}$ accumulation and ROS formation.** U-U937 (A,C,E,G) and D-U937 (B,D,F,H) cells were pretreated for 5 min with the vehicle, 2-APB, Ry or EN460 and incubated for 6 h with the further addition to arsenite. After treatments, the cells were analyzed for Fluo 4- (A,B), Rhod-2 (C,D), MitoSOX red-fluorescence (E,F), as well for ERO1α (G,H) protein expression. Anti-β-actin antibody was used to provide an internal loading control. The results represent the means ± S.D. calculated from at least three distinct experiments. (N.d., not detectable). *P <0.05; **P <0.01, as compared to untreated cells. (*) P <0.05; (**) P <0.01, as compared to cells treated with arsenite (ANOVA followed by Dunnett's test).

As mentioned above, U-U937 and D-C2C12 cells respond to arsenite with the release of $Ca^{2+}$ from the $IP_3R$ and the ensuing triggering of further $Ca^{2+}$ release from the RyR, critical for the mitochondrial accumulation of the cation and the resulting mito$O_2^{-\cdot}$ formation.

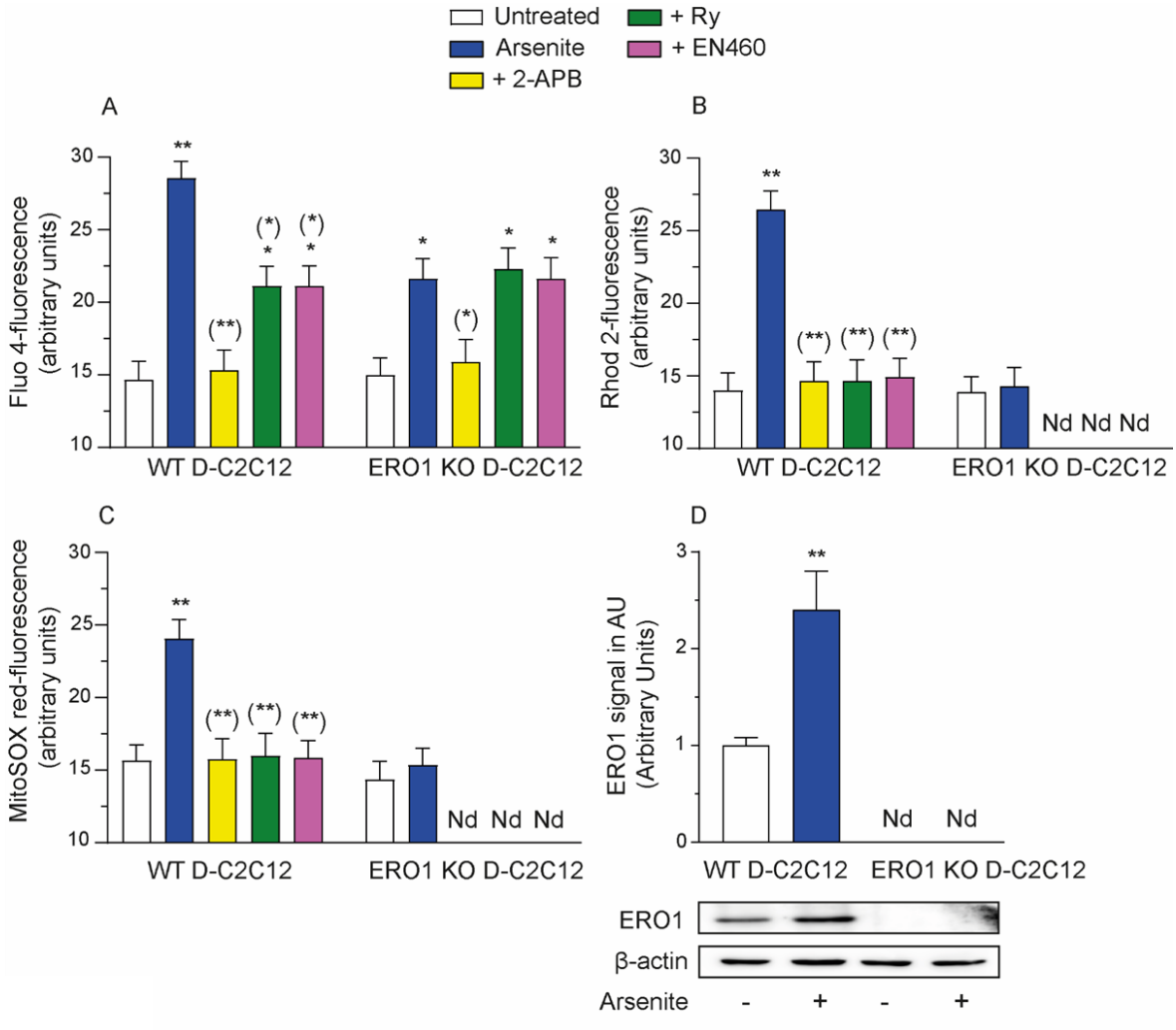


Unpublished data

**Fig. 17. Validation of the proposed mechanisms using ERO1α KO C2C12 Myotubes.** WT and ERO1α KO D-C2C12 cells were pretreated for 5 min with the vehicle, 2-APB, Ry or EN460 and incubated for 6 h with the further addition of arsenite. After treatments, the cells were analyzed for Fluo 4- (A), Rhod 2- (B) and MitoSOX red- (C) fluorescence. (D) Cells were incubated for 6 h in the absence or presence of arsenite and then analyzed for ERO1α protein expression. Anti-β-actin antibody was used as a loading control. The results represent the means ± S.D. calculated from at least three distinct experiments. (N.d., not detectable). *P <0.05; **P <0.01, as compared to untreated cells. (*) P < 0.05; (**) P <0.01, as compared to cells treated with arsenite (ANOVA followed by Dunnett's test).

These experiments were also performed in WT C2C12 myotubes (D-C2C12 cells) that responded to arsenite with a significant increase in $[Ca^{2+}]_c$ (Fig. 17A), $[Ca^{2+}]_m$ (Fig. 17B) and mito$O_2^{-\cdot}$ formation (Fig. 17C). 2-APB, Ry and EN460 produced effects in line with those observed in U-U937 cells.

On the other hand, arsenite induced a limited increase in $[Ca^{2+}]_c$ (Fig. 17A) in ERO1α KO D-C2C12 cells and this response was abolished by 2-APB and insensitive to Ry and EN460. In these cells, arsenite failed to promote mitochondrial $Ca^{2+}$ accumulation (Fig. 17B) and mito$O_2^{-\cdot}$ formation (Fig. 17C). Moreover, Western Blot analysis (Fig. 17D) provided evidence for enhanced ERO1α expression in WT D-C2C12 cells and for a lack of protein expression in the ERO1α KO counterpart.

In conclusion, the results reported in this section indicate that arsenite promotes mito$O_2^{-\cdot}$ formation *via* a mechanism in which the initial stimulation of the $IP_3R$, directly mediated by the metalloid, was followed by the triggering of a crosstalk between the $IP_3R$ and RyR. Importantly, RyR recruitment was critically regulated by the enhanced expression of ERO1α in turn associated with an ER stress response driven by the fraction of $Ca^{2+}$ released by the two channels. Thus, ERO1α plays a pivotal role in the regulation of processes associated with the mitochondrial $Ca^{2+}$ accumulation, and the ensuing mito$O_2^{-\cdot}$ formation, induced by arsenite.

# 4. Conclusions

Arsenite is a potent carcinogen producing an array of deleterious effects in target cells *via* its direct binding to protein thiols or indirectly, by promoting ROS formation through different mechanisms. We herein focused on the specific requirements and mechanism(s) mediating mito$O_2^{-\cdot}$ formation.

In our previous studies (Fiorani et al., 2018), we found that a critical event induced by arsenite in U-U937 cells, upstream to mito$O_2^{-\cdot}$ formation, is represented by its direct effects on the ER. More specifically, the metalloid caused an initial stimulation of the $IP_3R$ associated with the subsequent recruitment of the RyR and the ensuing mitochondrial $Ca^{2+}$ accumulation through the MCU. This last event was necessary but not sufficient for mito$O_2^{-\cdot}$ formation which, in order to take place, required additional effects of the metalloid on a mitochondrial target, most likely represented by the respiratory chain.

The first relevant information provided by the present work is that the direct effects in mitochondria require very short times of exposure to very low concentrations of arsenite. Indeed, when mitochondrial $Ca^{2+}$ accumulation was enforced with ATP or Cf, nanomolar concentrations of arsenite promoted mito$O_2^{-\cdot}$ formation after only a few min of exposure.

The time and concentration requirements for the induction of the effects of arsenite on the ER were instead remarkably longer/greater, as hours of exposure to micromolar levels of the metalloid were necessary to promote mitochondrial $Ca^{2+}$ accumulation.

An additional consideration on the effects of arsenite on the ER is related to the expression of the two major $Ca^{2+}$ channels, the $IP_3R$ and RyR, and their spatial relationship with mitochondria. Agonist studies provided functional evidence for the existence of close contact sites between the RyR and mitochondria, necessary to promote high [$Ca^{2+}$] microdomains nearby the

MCU, characterized by a low affinity for $Ca^{2+}$. We therefore observed that arsenite promotes mito$O_2^{-\cdot}$ formation in various cell types, expressing both the $IP_3R$ and RyR, regardless of whether undifferentiated or differentiated and hence also regardless of their proliferative status. In these cells, mito$O_2^{-\cdot}$ formation was associated with the time-dependent induction of mitochondrial dysfunction and apoptotic death.

Our results also indicate that arsenite fails to promote mitochondrial $Ca^{2+}$ accumulation in cell types uniquely expressing the $IP_3R$. It follows that, in these cells, the metalloid also fails to promote mito$O_2^{-\cdot}$ formation and the downstream toxic effects indicated above.

It is interesting to note that in these cells the $IP_3R$ was in close apposition with the mitochondria, as indicated by the results from experiments using $IP_3$-releasing agonists. The inability of arsenite to promote mitochondrial $Ca^{2+}$ accumulation is therefore likely due to the low $[Ca^{2+}]$ at the ER/mitochondria contact sites after $Ca^{2+}$ release from the $IP_3R$. The slow effects induced by the metalloid on the ER were indeed associated with an initial stimulation of the $IP_3R$ causing a limited release of $Ca^{2+}$. This fraction of the cation was nevertheless critical for the recruitment of the RyR and hence for the mitochondrial accumulation of the cation. In other words, arsenite promoted microdomains of high $[Ca^{2+}]$ required to allow MCU-dependent mitochondrial $Ca^{2+}$ uptake, exclusively nearby the RyR.

The phase of RyR recruitment is definitively critical in the process leading to arsenite-induced mito$O_2^{-\cdot}$ formation, and we have demonstrated that the crosstalk between the $IP_3R$ and RyR is regulated by ERO1α. The first evidence obtained in this direction was that ERO1α expression is increased under the same conditions in which arsenite induces $Ca^{2+}$ release from the $IP_3R$ and RyR. The second evidence was that EN460, which blunts the oxidase activity of ERO1α, recapitulated all the effects mediated by Ry. Finally, arsenite failed to recruit the RyR in ERO1α KO D-C2C12 cells, as

instead observed in ERO1α WT D-C2C12 cells. Thus, ERO1α promotes RyR recruitment after the initial $IP_3R$ stimulation induced by arsenite, which instead was independent on ERO1α activity/expression. $IP_3R$ activation induced by arsenite indeed takes place under conditions of low ERO1α expression.

We also determined that arsenite promotes ERO1α expression via a $Ca^{2+}$-dependent mechanism, in which both fractions of the cation, *i.e.* those derived from both the $IP_3R$ and RyR, are critically involved.

In the last part of the study, we performed experiments to identify the mechanism whereby arsenite enhances expression of ERO1α and obtained evidence for a role of $Ca^{2+}$ released from the both the $IP_3R$ and RyR. These results are therefore consistent with the possibility that the fraction of the cation released from the $IP_3R$ contributes to the ER stress response and CHOP accumulation, thereby enhancing the expression of its target protein ERO1α. In principle, the fraction of $Ca^{2+}$ released from the RyR may further enhance ERO1α expression by enforcing the above CHOP-dependent pathway, although mechanisms based on ROS formation should also be taken into consideration. RyR-derived $Ca^{2+}$ may indeed promote the formation of $mitoO_2^{-\cdot}$ and more specifically of its diffusible dismutation product, $H_2O_2$.

Thus, although more studies are required to fully understand this issue, we can nevertheless conclude that $Ca^{2+}$, regardless of whether released by the $IP_3R$ or RyR, indirectly promotes ERO1α expression. In this perspective, the arsenite-dependent ERO1α upregulation represents both a cause and a consequence of $Ca^{2+}$ release from the ER.

In conclusion, the results herein reported provide important information on the mechanism whereby arsenite promotes $mitoO_2^{-\cdot}$ formation. We identified two critical events, both necessary and non-sufficient, which the metalloid should induce in order to promote the formation of this species. The first one

is at level of the mitochondrial respiratory chain. Quite surprisingly, the metalloid induced its effects in a very short time and at very low concentrations. The second event instead occurred at the level of the ER and was associated with an initial release of $Ca^{2+}$ from the $IP_3R$, causing ER stress and CHOP-dependent ERO1α expression, critically connected with the recruitment of the RyR. The initial $IP_3R$-mediated $Ca^{2+}$ release is therefore responsible for the triggering of a positive feedback amplification mechanism resulting in ERO1α upregulation and ERO1α-dependent RyR activation which, besides providing a general increase in $[Ca^{2+}]_c$, and hence a further stimulation of ERO1α expression, critically mediates the enhanced $[Ca^{2+}]_m$ necessary for mito$O_2^{-\cdot}$ formation.

## 5. References

Abdul KS, Jayasinghe SS, Chandana EP, Jayasumana C, De Silva PM. Arsenic and human health effects: a review. Environ Toxicol Pharmacol. 40: 828-846. (2015).

Airey J, Baring M, Sutko J. Ryanodine receptor protein is expressed during differentiation in the muscle cell lines BC3H1 and C2C12 Dev. Biol. 148: 365-374. (1991).

Ambrosio F, Brown E, Stolz D, Ferrari R, Goodpaster B, Deasy B, Di Stefano G, Roperti A, Cheikhi A, Garciafigueroa Y, Barchowsky A. Arsenic induces sustained impairment of skeletal muscle and muscle progenitor cell ultrastructure and bioenergetics. Free Radic Biol Med. 74:64-73. (2014).

Bansaghi S, Golenar T, Madesh M, Csordas G, Ramachandrarao S, Sharma K, Yule DI, Joseph SK, Hajnoczky G. Isoform- and species-specific control of inositol 1,4,5-trisphosphate ($IP_3$) receptors by reactive oxygen species. J Biol Chem. 289:8170-8181. (2014).

Bennett DL, Cheek TR, Berridge MJ, De Smedt H, Parys JB, Missiaen L, Bootman MD. Expression and function of ryanodine receptors in nonexcitable cells. J Biol Chem. 271:6356-6362. (1996).

Berridge MJ. The inositol trisphosphate/calcium signaling pathway in health and disease. Physiol Rev (2016). 96:1261-1296. (2016).

Bootman M, Collins T, Peppiatt C, Prothero L, Mackenzie L, De Smet P, Travers M, Tovey S, T Seo, Berridge M, Ciccolini F, Lipp P. Calcium

signaling: an overview. Seminars in Cell & Developmental Biology. 12:3-10. (2012).

Brillantes AB, Ondrias K, Scott A, Kobrinsky E, Ondriasova E, Moschella MC, Jayaraman T, Landers M, Ehrlich BE & Marks AR. Stabilization of calcium release channel (ryanodine receptor) function by FK506-binding protein. Cell. 77(4):513-23. (1994).

Brillantes AM, Allen P, Takahashi T, Izumo S & Marks AR. Differences in cardiac calcium release channel (ryanodine receptor) expression in myocardium from patients with end-stage heart failure caused by ischemic versus dilated cardiomyopathy. Circ Res. 71(1):18-26. (1992).

Cantoni O, Guidarelli A. Indirect mechanisms of DNA strand scission by peroxynitrite. Methods Enzymol. 440:111-120. (2008).

Chernorudskiy AL and Zito E. Regulation of calcium homeostasis by ER redox: a close-up of the ER/mitochondria connection. J Mol Biol. 429(5):620-632. (2017).

Chou WC, Jie C, Kenedy AA, Jones RJ, Trush MA, and Dang CV. Role of NADPH oxidase in arsenic-induced reactive oxygen species formation and cytotoxicity in myeloid leukemia cells. Proc Natl Acad Sci USA. 101:4578-4583. (2004).

Clementi E, Guidarelli A, Cantoni O. The inositol 1,4,5-trisphosphate-generating agonist ATP enhances DNA cleavage induced by tert-butylhydroperoxide. Exp Cell Res. 239:175-178. (1998).

Delmotte P and Sieck GC. Interaction between endoplasmic/sarcoplasmic reticulum stress (ER/SR stress), mitochondrial signaling and $Ca^{2+}$ regulation in airway smooth muscle (ASM). Can J Physiol Pharmacol. 93:97-110. (2015).

Eisner V, Csordás G, and Hajnóczky G. Interactions between sarcoendoplasmic reticulum and mitochondria in cardiac and skeletal muscle – pivotal roles in $Ca^{2+}$ and reactive oxygen species signaling. J Cell Sci. 126:2965-2978. (2013).

Fauconnier J, Roberge S, Saint N, and Lacampagne A. Type 2 ryanodine receptor: a novel therapeutic target in myocardial ischemia/reperfusion. Pharmacol Ther. 138:323-332. (2013).

Fiorani M, Guidarelli A, Capellacci V, Cerioni L, Crinelli R, Cantoni O. The dual role of mitochondrial superoxide in arsenite toxicity: signaling at the boundary between apoptotic commitment and cytoprotection. Tox and Applied Pharmacol. 345:26-35. (2018).

Fitzgerald M, Neylon CB, Marks AR & Woodcock EA. Reduced ryanodine receptor content in isolated neonatal cardiomyocytes compared with the intact tissue. J Mol Cell Cardiol. 26(10):1261-5. (1994).

Flora SJ. Arsenic-induced oxidative stress and its reversibility. Free Radic Biol Med. 51:257-281. (2011).

Görlach A, Bertram K, Hudecova S, and Krizanova O. Calcium and ROS: a mutual interplay. Redox Biol. 6:260-271. (2015).

Guidarelli A, Cerioni L, Fiorani M, and Cantoni O. Differentiation-associated loss of ryanodine receptors: a strategy adopted by monocytes/macrophages to prevent the DNA single-strand breakage induced by peroxynitrite. J Immunol. 183:4449-4457. (2009).

Guidarelli A, Cerioni L, Fiorani M, Cantoni O. Differentiation-associated loss of ryanodine receptors: a strategy adopted by monocytes/macrophages to prevent the DNA single-strand breakage induced by peroxynitrite. J. Immunol. 183:4449-4457. (2009).

Guidarelli A, Cerioni L, Fiorani M, Catalani A, Cantoni O. Arsenite-induced mitochondrial superoxide formation: time and concentration requirements for the effects of the metalloid on the endoplasmic reticulum and mitochondria. J Pharmacol Exp Ther. 373:62-71. (2020).

Guidarelli A, Cerioni L, Tommasini I, Fiorani M, Brüne B, Cantoni O. Role of Bcl-2 in the arachidonate-mediated survival signaling preventing mitochondrial permeability transition-dependent U937 cell necrosis induced by peroxynitrite. Free Radic Biol Med. 39:1638-1649. (2005).

Guidarelli A, Fiorani M, Azzolini C, Cerioni L, Scotti M and Cantoni O. U937 cell apoptosis induced by arsenite is prevented by low concentrations of mitochondrial ascorbic acid with hardly any effect mediated by the cytosolic fraction of the vitamin. Biofactors. 41:101-110. (2015).

Guidarelli A, Fiorani M, Carloni S, Cerioni L, Balduini W and Cantoni O. The study of the mechanism of arsenite toxicity in respiration-deficient cells reveals that NADPH oxidase-derived superoxide promotes the same

downstream events mediated by mitochondrial superoxide in respiration-proficient cells. Toxicol Appl Pharmacol. 307:35-44. (2016).

Guidarelli A, Fiorani M, Cerioni L, Cantoni O. Calcium signals between the ryanodine receptor- and mitochondria critically regulate the effects of arsenite on mitochondrial superoxide formation and on the ensuing survival vs apoptotic signaling. Redox Biol. 20:285-295. (2019).

Guidarelli A, Fiorani M, Cerioni L, Cantoni O. The compartmentalized nature of the mechanisms governing superoxide formation and scavenging in cells exposed to arsenite. Toxicol Appl Pharmacol. 384:114-166. (2019).

Hakamata Y, Nakai J, Takeshima H & Imoto K. Primary structure and distribution of a novel ryanodine receptor/calcium release channel from rabbit brain. FEBS Lett 312(2-3):229-35. (1992).

Hirabayashi Y, Kwon SK, Paek H, Pernice WM, Paul MA, Lee J, Erfani P, Raczkowski A, Petrey DS, Pon LA, et al. ER-mitochondria tethering by PDZD8 regulates $Ca^{2+}$ dynamics in mammalian neurons. Science. 358:623-630. (2017).

Hosoi E, Nishizaki C, Gallagher KL, Wyre HW, Matsuo Y, Sei Y. Expression of the ryanodine receptor isoforms in immune cells. J Immunol. 167:4887-4894. (2001).

Hu Y, Li J, Lou B, Wu R, Wang G, Lu C, Wang H, Pi J, Xu Y. The Role of Reactive Oxygen Species in Arsenic Toxicity. Biomolecules. 10:240. (2020).

Jomova K, Jenisova Z, Feszterova M, Baros S, Liska J, Hudecova D, Rhodes CJ, Valko M. Arsenic: toxicity, oxidative stress and human disease. J Appl Toxicol. 31:95-107. (2011).

Kuwajima G, Futatsugi A, Niinobe M, Nakanishi S & Mikoshiba K. Two types of ryanodine receptors in mouse brain: skeletal muscle type exclusively in Purkinje cells and cardiac muscle type in various neurons. Neuron. 9(6):1133-42. (1992).

Liu SX, Davidson MM, Tang X, Walker WF, Athar M, Ivanov V, Hei TK. Mitochondrial damage mediates genotoxicity of arsenic in mammalian cells. Cancer Res. 65:3236-3242. (2005).

Marks AR, Priori S, Memmi M, Kontula K & Laitinen PJ. Involvement of the cardiac ryanodine receptor/calcium release channel in catecholaminergic polymorphic ventricular tachycardia. J Cell Physiol. 190:1-6. (2002).

Marks AR, Tempst P, Hwang KS, Taubman MB, Inui M, Chadwick C, Fleischer S & Nadal-Ginard B. Molecular cloning and characterization of the ryanodine receptor/junctional channel complex cDNA from skeletal muscle sarcoplasmic reticulum. Proc Natl Acad Sci USA. 86(22):8683-7. (1989).

Marx SO, Reiken S, Hisamatsu Y, Gaburjakova M, Gaburjakova J, Yang YM, Rosemblit N & Marks AR. Phosphorylation-dependent regulation of ryanodine receptors: a novel role for leucine/isoleucine zippers. J Cell Biol 153(4):699-708. (2001).

Marx SO, Reiken S, Hisamatsu Y, Jayaraman T, Burkhoff D, Rosemblit N & Marks AR. PKA phosphorylation dissociates FKBP12.6 from the calcium release channel (ryanodine receptor): defective regulation in failing hearts. Cell. 101(4):365-76. (2000).

McPherson PS & Campbell KP. Solubilization and biochemical characterization of the high affinity [3H] ryanodine receptor from rabbit brain membranes. J Biol Chem. 265(30):18454-60. (1990).

Moschella MC, Watras J, Jayaraman T & Marks AR. Inositol 1,4,5-trisphosphate receptor in skeletal muscle: differential expression in myofibres. J Muscle Res Cell Motil. 16(4):390-400. (1995).

Raffaello A, Mammucari C, Gherardi G, and Rizzuto R. Calcium at the center of cell signaling interplay between endoplasmic reticulum, mitochondria, and lysosomes. Trends Biochem Sci. 41:1035-1049. (2016).

Rizzuto R, De Stefani D, Raffaello A, Mammucari C. Mitochondria as sensors and regulators of calcium signaling. Nat Rev Mol Cell Biol. 13:566-578. (2012).

Rosemblit N, Moschella MC, Ondriasova E, Gutstein DE, Ondrias K & Marks AR. Intracellular calcium release channel expression during embryogenesis. Dev Biol. 595(10):3041–3051. (1999).

Sankpal UT, Pius H, Khan M, Shukoor MI, Maliakal P, Lee CM, Abdelrahim M, Connelly SF, and Basha R. Environmental factors in causing human cancers: emphasis on tumorigenesis. Tumor Biol. 33:1265-1274. (2012).

Shakoor MB, Nawaz R, Hussain F, Raza M, Ali S, Rizwan M, Oh SE, and Ahmad S. Human health implications, risk assessment and remediation of As-contaminated water: a critical review. Sci Total Environ. 601, 602:756-769. (2017).

Straub AC, Clark KA, Ross MA, Chandra AG, Li S, Gao X, Pagano PJ, Stolz DB, Barchowsky A. Arsenic-stimulated liver sinusoidal capillarization in mice requires NADPH oxidase-generated superoxide. J Clin Invest. 118:3980-3989. (2008).

Sugiyama T, Yamamoto-Hino M, Miyawaki A, Furuichi T, Mikoshiba K, Hasegawa M. Subtypes of inositol 1,4,5-trisphosphate receptor in human hematopoietic cell lines: dynamic aspects of their cell-type specific expression. FEBS Lett. 349:191-196. (1994).

Sukhvinder K, Majid RK and Arif A. Role of arsenic and its resistance in nature. Can J Microbiol. 57:10. (2011).

Sun H, Yang Y, Shao H, Sun W, Gu M, Wang H, Jiang L, Qu L, Sun D, Gao Y. Sodium Arsenite-induced learning and memory impairment is associated with endoplasmic reticulum stress-mediated apoptosis in rat hippocampus. Front Mol Neurosci. 10: 286. (2017).

Varone E, Pozzer D, Di Modica S, Chernorudskiy A, Nogara L, Baraldo M, Cinquanta M, Fumagalli S, Villar-Quiles R N, De Simoni M. G., Blaauw B, Ferreiro A & Zito E. SELENON (SEPN1) protects skeletal muscle from saturated fatty acid-induced ER stress and insulin resistance. Redox Biol. 24:101-176. (2019).

Zalk R, Clarke OB, Des Georges A, Grassucci RA, Reiken S, Mancia F, Hendrickson WA, Frank J & Marks AR. Structure of a mammalian ryanodine receptor. Nature. 517(7532):44-9. (2015).

Zito E, Chin K. T, Blais J, Harding H. P. & Ron D. ERO1-beta, a pancreas-specific disulfide oxidase, promotes insulin biogenesis and glucose homeostasis. J Cell Biol. 188:821-32. (2010).